Evolutionary unique *N*-glycan-dependent protein quality control system plays pivotal roles in cellular fitness and extracellular vesicle transport in *Cryptococcus neoformans*

Catia Mota[1], Kiseung Kim[1], Ye Ji Son[1], Eun Jung Thak[1], Su-Bin Lee[1], Ju-El Kim[2], Jeong-Kee Yoon[2], Min-Ho Kang[3,4], Heeyoun Hwang[5], Yong-Sun Bahn[6], J. Andrew Alspaugh[7], and Hyun Ah Kang[1*]

[1] Department of Life Science, Chung-Ang University, Seoul, 06974, Republic of Korea

[2] Department of Systems Biotechnology, Chung-Ang University, Anseong-Si, Gyeonggi-Do, 17546, Republic of Korea

[3] Department of Biomedical-Chemical Engineering, The Catholic University of Korea, Bucheon-Si, 14662, Republic of Korea

[4] Department of Biotechnology, The Catholic University of Korea, Bucheon-Si, 14662, Republic of Korea

[5] Digital OMICs Research Center, Korea Basic Science Institute, Cheongju-si, 28119, Republic of Korea

[6] Department of Biotechnology, Yonsei University, Seoul, 03722, Republic of Korea

[7] Department of Medicine, Duke University, Durham, North Carolina, USA

*For correspondence (H. A. K.) E-mail: hyunkang@cau.ac.kr; Tel.: +82-2-820-5863; Fax: +82-2-825-5206

Abstract

A conserved *N*-glycan-dependent endoplasmic reticulum protein quality control (ERQC) system has evolved in eukaryotes to ensure accuracy during glycoprotein folding. The human pathogen *Cryptococcus neoformans* possesses a unique *N*-glycosylation pathway that affects microbial physiology and interactions with the infected host. To investigate the molecular features and functions of the ERQC system in *C. neoformans*, we characterized a set of mutants with deletion of genes coding for the ERQC sensor UDP-glucose:glycoprotein glucosyltransferase (*UGG1*) and putative α1,2-mannose-trimming enzymes (*MNS1*, *MNS101*, *MNL1*, and *MNL2*). The *ugg1*Δ, *mns1*Δ, *mns101*Δ, and *mns1*Δ*101*Δ mutants showed alterations in *N*-glycan profiles, defective cell surface organization, decreased survival in host cells, and varying degrees of reduced *in vivo* virulence. The *ugg1*Δ strain exhibited severely impaired extracellular secretion of capsular polysaccharides and virulence-related enzymes. Comparative transcriptome analysis showed the upregulation of protein folding, proteolysis, and cell wall remodeling genes, indicative of induced ER stress. However, no apparent changes were observed in the expression of genes involved in protein secretion or capsule biosynthesis. Additionally, extracellular vesicle (EV) analysis combined with proteomic analysis showed significant alterations in the number, size distribution, and cargo composition of EVs in *ugg1*Δ. These findings highlight the essential role of the functional ERQC system for cellular fitness under adverse conditions and proper EV-mediated transport of virulence factors, which are crucial for the full fungal pathogenicity of *C. neoformans*.

Keywords: *Cryptococcus neoformans*, glycoprotein quality control, UDP-glucose: glycoprotein glucosyltransferase, extracellular vesicles, pathogenicity

Introduction

Glycoproteins, destined for the secretory pathways, enter the endoplasmic reticulum (ER) lumen where protein folding occurs (Rapoport, 2007). The accumulation of misfolded proteins affects cell viability and homeostasis; therefore, eukaryotes evolved a conserved ER quality control (ERQC) system that recognizes folding defects, repairs them, or ensures the translocation of irreparable misfolded proteins into the cytosol for proteasome-mediated degradation via the ER-associated degradation (ERAD) system (Thibault and Ng, 2012; Xu and Ng, 2015; Balchin et al., 2016), a process that heavily relies on *N*-glycosylationto determine protein folding conformation (Aebi, 2013; Varki, 2017).

Many aspects of *N*-glycosylation are highly conserved, and most eukaryotes initiate this process by synthesizing a Dol-PP-linked $Glc_3Man_9GlcNAc_2$ oligosaccharide as a common core *N*-glycan, which attaches to nascent polypeptides in the ER via an asparagine residue. Glucosidases I and II (Gls1 and Gls2) remove two glucose residues from the core oligosaccharide. Proteins containing monoglucosylated *N*-glycans ($Glc_1Man_9GlcNAc_2$) enter a calnexin and/or calreticulin (CNX/CRT in mammals; Cne in yeast) chaperone-mediated folding cycle. Finally, Gls2 cleaves the remaining glucose residue. If proteins are misfolded, they are recognized by the ERQC checkpoint enzyme UDP-glucose:glycoprotein glucosyltransferase (UGGT), which reglucosylates them for re-entry into the folding cycle (Fig. 1A). Then, the *N*-glycans of the accurately folded proteins are further processed by Gls2 and α1,2-mannosidase I (Mns1) and moved to the Golgi apparatus. However, irreparably misfolded glycoproteins are targeted for ERAD, where they undergo demannosylation and retro-translocation for proteasomal degradation in the cytosol. Recently, *N*-glycan precursors in the ER of some protists and fungi were found to be shorter than the typical 14-sugar *N*-glycan precursors in most eukaryote organisms. The length of these *N*-glycan precursors significantly impacts *N*-glycan-dependent QC of glycoprotein folding and ERAD (Banerjee

et al., 2007; Samuelson et al., 2015).

The basidiomycetous fungus *Cryptococcus neoformans* is an opportunistic encapsulated human pathogen that primarily affects immunocompromised individuals, causing fatal meningoencephalitis (Gottfredsson and Perfect, 2000; Kwon-Chung et al., 2000). The *N*-glycosylation pathway of *C. neoformans* is evolutionarily conserved; nevertheless, the structure and biosynthesis of its *N*-glycans includes several unique features (Park et al., 2012). *C. neoformans* contains serotype-specific high-mannose-type *N*-glycans with or without a β-1,2-xylose residue attached to the trimannosyl core. Additionally, acidic *N*-glycans of *C. neoformans* contain xylose phosphates attached to the mannose residues both within the *N*-glycan core and outer mannose chains. The intact core *N*-glycan structure is crucial for *C. neoformans* pathogenicity (Thak et al., 2020); hence, alterations in the *N*-glycan structure modulates the interaction between the cell surface mannoproteins and host cells (Lee et al., 2023). Additionally, *C. neoformans* lacks homologous genes to the Asn-Linked Glycosylation (ALG) genes *ALG6*, *ALG8*, and *ALG10*, which are evolutionary conserved across most eukaryotic organisms and encode the glucosyltransferases that add the glucose residues to the core *N*-glycan before its attachment to proteins (Park et al., 2012). $Man_7GlcNAc_2$ and $Man_8GlcNAc_2$ without glucose residues are primarily detected in Dol-PP-linked glycans of *C. neoformans* (Samuelson et al., 2005). Moreover, the mature core *N*-glycan structures assembled on the cell surface mannoproteins of *C. neoformans* are primarily $Man_{6–7}GlcNAc_2$, which are shorter than the expected $Man_8GlcNac_2$ (Park et al., 2012). This observation led to the speculation that the terminal α-1,2-mannose residues of *C. neoformans* *N*-linked glycans may be more susceptible to trimming by ER α-1,2 mannosidases due to the lack of glucose residues compared to most eukaryotes. Alternatively, the presence of multiple α-1,2 mannosidases may generate more extensively trimmed core *N*-glycans in *C. neoformans*.

C. neoformans employs several virulence factors, including an extensive polysaccharide capsule composed of glucuronoxylomannan (GXM) and galactoxylomannan (GXMGal) (Doering et al., 2009), melanin (Qiu et al., 2012), and various extracellular enzymes such as phosphatase and urease (Singh et al., 2013), all of which contribute to immune evasion and enhance fungal pathogenicity. To facilitate the export of these virulence-associated molecules, *C. neoformans* employs both conventional (Yoneda and Doering, 2006; Panepinto et al., 2009) and unconventional secretion pathways (Rodrigues et al., 2007; Casadevall et al., 2019; Rizzo et al., 2021). Classical secretion relies on the ER-Golgi network, while non-classical mechanisms, such as extracellular vesicle (EV)-mediated transport, provide an alternative route for cargo delivery beyond the conventional secretory pathway. *C. neoformans* EVs have been described as a heterogeneous population of "virulence bags" containing numerous fungal survival and pathogenicity-associated cargo. Proteomic analyses of EV cargo have identified several cell surface glycoproteins, including members of the CDA family, well-known immunomodulators (Spetch et al., 2017; Rizzo et al., 2021). The ERQC system is essential for maintaining protein homeostasis by ensuring proper folding, glycosylation, and directed trafficking of secreted proteins to downstream compartments within the conventional secretory pathway. Defects in ERQC affect the fidelity of protein secretion not only by accumulation or degradation of misfolded proteins, leading to the impaired secretion of functional proteins, but also by the escape of misfolded forms, thus resulting in increased secretion of non-properly processed proteins (Marcus and Perlmutter, 2000; Chen et al., 2024). However, the potential of ERQC to modulate EV-mediated protein trafficking is not yet systematically investigated.

This study presents the first systematic analysis of *N*-glycan-dependent ERQC in *C. neoformans* using mutant strains lacking ERQC gene homologs. Our findings highlight the

critical roles of ERQC in maintaining cellular fitness and facilitating EV-mediated transport of virulence factors.

Results

Evolutionary unique features of *C. neoformans* ERQC components

We performed BLAST analysis of the *C. neoformans* H99 genome to identify the ERQC pathway-associated homologous genes of *C. neoformans*, followed by comparison with the ERQC components in other eukaryotic organisms (Supplementary Fig. S1, A). Unlike most eukaryotes, several yeast species within the Ascomycota phylum, such as *Saccharomyces cerevisiae* and *Candida albicans*, do not possess a functional UGGT. In contrast, UGGT homologs were identified in most Basidiomycota fungal species, including *C. neoformans* (Supplementary Fig. S1, A and B). The *C. neoformans* UGGT (CNAG_03648), which has been named as Ugg1, consists of 1,582 amino acids (aa) and features a signal peptide (1–20 aa) along with four tandem-like thioredoxin-like (TRXL) domains: TRXL12 (33–320 aa), TRXL13 (28–416 aa), TRXL14 (432–618 aa), and TRXL15 (712–950 aa). Ugg1 also contains a glucosyltransferase (GT) 24 domain with a DXD motif (1,369–1,371 aa), and a KDEL-like ER retention signal (1579–1582 aa), which facilitates its retrieval from the Golgi apparatus (Fig. 1B, Supplementary Fig. S2, A).

Additionally, we identified two *C. neoformans* ORFs, Mns1 (CNAG_02081) and Mns101 (CNAG_03240), as homologs of the eukaryote α1,2-mannosidase I, which processes *N*-glycans before exporting them to the Golgi. The *C. neoformans* Mns1 and Mns101 show 42.4% and 28.8% amino acid identities to *S. cerevisiae* ER α1,2-mannosidase I, respectively, and share 30.9% identity between them. Furthermore, *C. neoformans* Mnl1 (CNAG_01987) and Mnl2 (CNAG_04498) were identified as putative components of ERQC in *C. neoformans* (Supplementary Fig. S1, A and C). *C. neoformans* Mnl1 is a homolog of the yeast α1,2-mannosidase-like protein Htm1, which processes *N*-glycans targeted for ERAD. In contrast, *C. neoformans* Mnl2 encodes a mannosidase that does not share significant

similarity with mannosidases from other eukaryotes. Mns1, Mns101, and Mnl1 possess glucosyl hydrolase (GH) 47 domains, essential for mannosidase activity, whereas Mnl2 contains a GH92 domain, also associated with mannosidase activity (Fig. 1B). The Mns1 and Mnl1 families are characterized by conserved cysteine (Cys) and alanine (Ala) residues within their activity domains, as previously described (Jakob et al., 2001). These conserved residues are present in *C. neoformans* Mns1, Mns101, and Mnl1 but are absent in Mnl2 (Supplementary Fig. S2, B). Notably, Mns101 and Mnl2 are Basidiomycota-specific proteins (Supplementary Fig. S1, A) and appear to have diverged early from other fungal mannosidase clades based on phylogenetic analysis (Supplementary Fig. S1, C). Interestingly, neither Mnl1 nor Mnl2 contains canonical KDEL/HDEL-like ER retention signals. In *S. cerevisiae*, the ER retention of Mnl1/Htm1 is mediated through its interaction with protein disulfide isomerase Pdi1, which carries an HDEL sequence (Gauss et al., 2011). Similarly, *C. neoformans* Mnl1 and Mnl2 may employ a non-canonical retention mechanism, likely facilitated by interactions with other ER-resident proteins, to achieve ER localization.

Loss of *UGG1*, *MNS1*, and *MNS101* causes alteration of *N*-glycan profiles in *C. neoformans*

We performed high-performance liquid chromatography (HPLC) analysis of the cell wall mannoproteins (cwMPs) from both the wild-type (WT) and ERQC mutant strains to investigate the ERQC malfunction-induced structural differences in *N*-glycans (Fig. 2). The HPLC profiles of cwMPs from the WT strain showed an M8 peak as the major species. This peak corresponded to *N*-glycans with 8 mannose residues (Fig. 2A, top). The glycan structure at the M8 peak ($Man_8GlcNAc_2$) in the WT primarily corresponded to the $Man_7GlcNAc_2$ core *N*-glycan with an additional mannose residue that is linked via an α1,6-linkage and added in

the Golgi apparatus (Park et al., 2012). In the *ugg1*Δ mutant, M8 was also the main *N*-glycan species, but the pools of hypermannosylated *N*-glycans (larger than the M11 peak) were markedly reduced (Fig. 2A, middle). The altered *N*-glycan profile of the *ugg1*Δ mutant was restored to that of the WT after complementation with the WT *UGG1* gene (Fig. 2A, bottom). The lectin blotting analysis using *Galanthus nivalis* agglutinin (GNA), which specifically binds to terminal α1,2-, α1,3-, and α1,6-linked mannose residues, showed a distinctive increase of glycoproteins with lower molecular weight in the secretory proteins in *ugg1*Δ compared to those in WT (Fig. 2B). This observation aligns with the decrease of hypermannosylated *N*-glycans in the *ugg1*Δ mutant. Overall, these results suggest that Ugg1 is involved in mediating the hypermannosylation of *N*-glycans in the Golgi apparatus.

We also assessed putative α1,2-mannosidase I genes for roles in protein mannosylation. The *mns1*Δ mutant *N*-glycan profile showed a peak shift from an M8 to an M9 form, which strongly indicates that *C. neoformans* Mns1 could be the primary ER α1,2-mannosidase I (Fig. 2C, *mns1*Δ). Notably, the loss of Mns101, which is present only in Basidiomycota, increased the fractions containing hypermannosylated glycans (> M10) while maintaining M8 as a primary core *N*-glycan form. This suggests that the basidiomycete-specific Mns101 may potentially be a novel α1,2-mannosidase that functions to remove mannose residues from hypermannosylated *N*-glycans in the Golgi apparatus or further trims the M8 glycan in the ER before the glycoproteins are transported to the Golgi (Fig. 2C, *mns101*Δ). The matrix-assisted laser desorption ionization-time of flight (MALDI-TOF) mass spectrometer analysis of neutral *N*-glycans (Fig. 2C), further confirmed the shift of the major M8 peak in the WT strain to M9 in the *mns1*Δ mutant and the increase in the hypermannosylation profile in the *mns101*Δ mutant (Fig. 2D). The *N*-glycan profiles of the *mns1*Δ*101*Δ double mutant showed the combined effect of each null mutation, and it showed both increased hypermannosylated glycans and a shift from the M8 to the M9 peak in both

the HPLC (Fig. 2C, *mns1*Δ*101*Δ) and MALDI-TOF analyses. This indicates that Mns1 and Mns101 serve as mannosidases and play independent roles at different stages of *N*-glycan processing in *C. neoformans*.

In contrast, the loss of both *MNL1* and *MNL2* did not show notable differences in the HPLC profile of *N*-glycans from cell surface mannoproteins (Supplementary Fig. S3, A). Considering the expected function of Mnl1 and Mnl2 in ERAD, their substrates are likely misfolded proteins that have not been transported to the Golgi apparatus. Thus, we speculate that only the normally processed *N*-glycan profiles of cell surface mannoproteins in the *mnl1*Δ *mnl2*Δ mutant strain were observed.

Loss of ERQC components results in defective growth fitness and increased stress sensitivity

To investigate the changes in ERQC-related gene expression under stress conditions, we conducted quantitative reverse transcription PCR (qRT-PCR) analysis of *C. neoformans* following treatment with tunicamycin (TM, 5 μg/ml), a well-established inhibitor of *N*-glycosylation, or dithiothreitol (DTT, 20 mM), which disrupts disulfide bond formation and induces the accumulation of misfolded proteins. Additionally, we examined gene expression after growth at 37 °C (Fig. 3A). When misfolded proteins accumulate in the ER, the unfolded protein response (UPR) system is activated to restore homeostasis (Chakraborty et al., 2016). As expected, *KAR2*, encoding a molecular chaperone associated with the UPR system, was upregulated in response to TM treatment, DTT treatment, and heat stress at 37 °C. The ERQC components *UGG1*, *MNS1*, *MNS101*, *MNL1*, and *MNL2* were upregulated by DTT treatment; however, only *UGG1* was slightly induced following TM treatment. The high-temperature conditions also induced the expression of *KAR2*, *UGG1* and *MNL2*. Notably, DTT treatment

221 induced a 10-fold higher expression of *MNS1* and *MNL1*. These results strongly suggest that
222 the *C. neoformans* genes *UGG1*, *MNS1*, *MNS101*, *MNL1*, and *MNL2* are crucial components
223 of the ERQC and ERAD systems, although each respond uniquely to various cell/ER stress
224 conditions.

225 We next investigated the growth of the *ugg1*Δ mutant under various stress-inducing
226 conditions to elucidate the roles of the ERQC components in ER stress response and
227 adaptation, which are closely associated with *C. neoformans* virulence. The *ugg1*Δ mutant
228 showed impaired growth even under normal growth conditions (Fig. 3B) and increased
229 sensitivity to ER stress-inducing agents such as DTT, TM and cell wall stressors, including as
230 calcofluor white (CFW), congo red (CR), sodium dodecyl sulfate (SDS), and caffeine.
231 Additionally, *ugg1*Δ showed hindered growth in the presence of antifungal drugs such as
232 azole agents (fluconazole and ketoconazole) and the glucose transport inhibitor fludioxonil.
233 These findings suggest that Ugg1 is crucial for the robust growth and survival of *C.*
234 *neoformans* under various stress conditions. In contrast, the single deletion (*mns1*Δ and
235 *mns101*Δ) and double deletion *(mns1*Δ*101*Δ) strains did not exhibit noticeable phenotypic
236 changes except for a slight increase in sensitivity of *mns101*Δ and *mns1*Δ*101*Δ to higher
237 fludioxonil concentrations (Supplementary Fig. S3, B). Similarly, neither the single nor
238 double disruption of *MNL1* and *MNL2* produced detectable changes in the tested growth
239 conditions (Supplementary Fig. S3, C).

240 Amino acid analogues have been used for evaluating the functionality of protein
241 folding, as its incorporation into newly synthesized proteins interrupts proper protein folding
242 (Trotter et al., 2002; Cowie et al., 1959). We hypothesized that, in the context of a defective
243 ERQC pathway, misfolded proteins cannot be adequately repaired and accumulate, thus
244 triggering ER stress, which may ultimately inhibit cell growth in the presence of amino acid
245 analogues. In the presence of the leucine analogue 5',5',5'-trifluoroleucine (TFL), *ugg1*Δ

showed noticeably inhibited growth, whereas the WT strain showed no growth inhibition (Fig. 3C). The *mns1*Δ*101*Δ strain also exhibited slightly increased sensitivity to TFL compared with that of the WT strain.

As a defense mechanism against misfolded protein accumulation-mediated ER stress, UPR is induced by the unconventional splicing of the *HXL1* transcription factor in *C. neoformans* (Cheon et al., 2011). RT-PCR analysis revealed a significantly elevated level of spliced *HXL1* in the *ugg1*Δ strain compared to the WT, even under normal culture conditions (Fig. 3D), strongly indicating that the loss of *UGG1* leads to the accumulation of misfolded proteins, triggering ER stress under standard growth conditions. Furthermore, green fluorescence protein (GFP)-tagged Ugg1, Mns1, and Mns101 proteins colocalized with the ER marker, supporting their role as confirming them to be functional ERQC components based on their subcellular localization in the ER (Supplementary Fig. S4).

ERQC defects lead to virulence attenuation in *C. neoformans*

We investigated the effects of a defective ERQC on *in vitro* virulence phenotypes of *C. neoformans* by analyzing capsule and melanin production, as these are two of the major virulence factors of *C. neoformans*. Culturing on L-DOPA-containing plates showed that melanin production was reduced in the *ugg1*Δ strain compared with that in the WT (Fig. 4A, top), whereas the *mns1*Δ*101*Δ mutant cells did not show detectable defects at either 30 or 37 °C (Fig. 4A, bottom). Considering the decreased growth of the *ugg1*Δ strain, the melanin production of *C. neoformans* cells cultivated in liquid L-DOPA was measured and normalized by cell density, which further confirmed the decreased melanin production activity of the *ugg1*Δ strain (Fig. 4B). India ink staining of the capsule showed significantly reduced capsule thickness in the *ugg1*Δ strain and a moderate defect in the *mns1*Δ*101*Δ strain (Fig. 4C).

Defects in the ERQC system led to a more apparent decrease in pathogenicity in a murine model of systemic cryptococcosis. Notably, the *ugg1*Δ strain was almost avirulent with no detectable signs of illness in the infected animals (Fig 4D). Although *MNS1* and *MNS101* single disruptions did not cause a detectable decrease in *C. neoformans* pathogenicity, their double disruption resulted in decreased virulence. Histopathological analysis of infected mice lungs suggested significantly reduced lung colonization by both *ugg1*Δ and *mns1*Δ*101*Δ cells (Supplementary Fig. S5, A). Additionally, the fungal burden of *ugg1*Δ-infected animals showed a notable decrease in organ colonization at 60 days post-infection (dpi) (Supplementary Fig. S5, B). Analysis of the fungal burden at 7 dpi showed significantly reduced organ colonization of the *mns1*Δ*101*Δ mutant compared with that of the WT (Supplementary Fig. S5, C). Consistent with the *in vivo* survival data, the number of surviving *ugg1*Δ and *mns1*Δ*101*Δ cells within the macrophage-like cell line J447A.1 was significantly lower compared with that of the WT strain (Fig. 4E). These data suggest that a functional ERQC system is critical for maintaining full *in vivo* pathogenicity and ensuring robust survival within host immune cells.

Loss of Ugg1 function manifests defects in extracellular transport of GXM

Cryptococcal capsule materials are synthesized intracellularly and secreted to the cell surface. Subsequently, they are assembled and bound to the cell wall (Yoneda and Doering, 2006). The observed capsule defects in the *ugg1*Δ and *mns1*Δ*101*Δ mutant strains may be attributed to issues in the capsule polysaccharide synthesis or transport steps. Alternatively, defective capsule formation could arise from an increased shedding of capsule polymers, preventing their proper attachment to the cell surface. To determine the cause of the capsule defects, we examined the amounts of capsular polysaccharides synthesized intracellularly and

294 those shed into the culture supernatant by a capsule blotting assay, using the 18B7 antibody
295 directed against GXM, the major capsule component (Casadevall et al., 1998). As controls,
296 we also tested capsule production and secretion in the *cap59*Δ strain with a defect in GXM
297 synthesis (Grijpstra et al., 2009) and the *rim101*Δ strain with a capsule attachment defect
298 despite normal polysaccharide synthesis and secretion (O'Meara et al., 2010). Intracellular
299 GXM quantities did not notably differ between the WT, *ugg1*Δ, *mns1*Δ*101*Δ, and *rim101*Δ
300 strains, although *ugg1*Δ showed slightly reduced GXM level (Fig. 5A, left). In contrast, no
301 intracellular GXM was detected in *cap59*Δ, which was consistent with its defect in GXM
302 synthesis. Moreover, the *ugg1*Δ strain was defective in capsule polymer secretion/shedding,
303 whereas the *mns1*Δ*101*Δ strain displayed enhanced shedding of GXM-containing polymers
304 that appeared to be shorter in length than the WT-type polymers, suggestive of poor
305 polysaccharide polymerization (Fig. 5A, right). Therefore, these results suggest that *ugg1*Δ
306 contains a defect in polysaccharide trafficking to the extracellular space, whereas *mns1*Δ*101*Δ
307 has a defect in polysaccharide polymerization, resulting in defective capsule elaboration,
308 albeit with differential degrees of severity in both ERQC mutants.

309 Furthermore, to determine whether the ERQC mutants are also impaired in capsule
310 attachment, we performed a capsule transfer assay, to assess whether exogenously shed
311 capsule polysaccharides can bind to acapsular mutants (Reese and Doering, 2003). The
312 hypocapsular *rim101*Δ mutant did not show reassociation of capsular polysaccharides;
313 however, the acapsular *cap59*Δ mutant showed recovery of capsule formation when co-
314 incubated with exogenous GXM (Fig. 5B). Similarly, *ugg1*Δ reverted its acapsular phenotype
315 on incubation with the WT-shed polysaccharides, strongly suggesting that the defective
316 capsule phenotype of *ugg1*Δ is primarily due to defective GXM secretion rather than
317 impaired attachment of capsule polymers. We further conducted a capsule transfer assay
318 using capsular polysaccharides shed from *mns1*Δ*101*Δ. The *cap59*Δ mutant reverted to the

capsular phenotype by attaching to the *mns1*Δ*101*Δ-shed polymers. However, the fluorescence intensity of the capsule generated was significantly lower than that of the cells attached with polysaccharides obtained from the WT. Although the decreased length of capsule polysaccharides should be validated by techniques specifically measuring GXM size (De Jesus et al., 2010), this result suggests that the *mns1*Δ*101*Δ double mutant secretes incomplete capsule polysaccharides (Fig. 5C), leading to a hypocapsular phenotype. These results collectively indicate that disrupting the ERQC results in impaired capsule formation by defective GXM trafficking to the extracellular space.

Transmission electron microscopy (TEM) imaging of the WT and mutant cells distinctly showed a diminished capsule structure and loss of capsule shedding in the *ugg1*Δ strain compared with that of the WT strain (Fig. 5D). Additionally, we observed considerable thinning of the cell walls in both ERQC mutant cells. Notable changes in intracellular structures along with an increase in the number of pigmented vesicles were observed in the mutant cells even under YPD culture conditions. Under capsule-inducing conditions, a significant accumulation of vesicular structures (electron-lucent structures) was observed intracellularly, particularly in *ugg1*Δ. We performed lipid droplet (LD) staining to determine whether these vesicular structures might be LDs. We observed a notable increase in LDs in *ugg1*Δ under capsule-inducing culture conditions (Supplementary Fig. S6, A). LDs impact proteostasis by sequestering misfolded proteins intended for degradation and providing an "escape hatch" when the ERQC is overloaded (Ploegh, 2007; Vevea et al., 2015). Additionally, FM4-64 dye staining showed increased number of vacuoles in the *ugg1*Δ cells compared with that in the WT (Supplementary Fig. S6, B). Moreover, all the observed abnormal phenotypes were less pronounced in the *mns1*Δ*101*Δ mutant than in the *ugg1*Δ strain. Collectively, the altered vesicular structures observed in the *ugg1*Δ and *mns1*Δ*101*Δ strains highlight the critical role of ERQC in maintaining proper vesicular architecture and

cell surface organization. These functions are tightly linked to extracellular trafficking of virulence factors and cell wall remodeling.

***ugg1*Δ transcriptomic profiling shows induced ER and cell wall integrity stress responses**

To elucidate the mechanisms underlying *UGG1* deletion-induced physiological changes in *C. neoformans*, we performed RNA sequencing (RNAseq)-based transcriptome analysis of the WT and *ugg1*Δ strains under standard growth conditions (YPD medium, 30 °C). Comparative transcriptome analysis showed statistically significant alterations exceeding 2-fold in the expression patterns of 146 genes, of which 85 were upregulated and 61 were downregulated compared with that of the WT strain (Fig. 6A, B, Supplementary Tables S2, A and B).

Notably, the *ugg1*Δ mutant showed upregulation of genes such as *SKN1* and *KRE6* (transmembrane glucosidases involved in the sphingolipid biosynthesis and β-glucan biosynthesis), *CAT2* (a putative peroxisomal catalase), *CHS7* (chitin synthase export chaperone), and CNAG_05458 (a putative endo-1,3(4)-β-glucanase). In contrast, genes encoding *ERG3* and *ERG25* (associated with the ergosterol biosynthesis pathway) and *FHB1* (flavohemoglobin denitrosylase associated with counteracting nitric oxide stress) were significantly downregulated. Gene Ontology (GO) analysis in *ugg1*Δ showed pronounced induction of genes implicated in various cellular processes, including the hydrolysis of *O*-glycosyl compounds for cell wall remodeling, DNA replication, proteolysis, ribosome biogenesis, protein folding, and serine/threonine kinase activity. In contrast, genes associated with carbohydrate and lipid metabolism, chaperone binding, iron homeostasis, and mitochondrial intermembrane space were considerably downregulated (Fig. 6C). The

transcriptome profile strongly suggests that loss of Ugg1 function induces the expression of several genes involved in maintaining cell wall integrity to compensate for cell wall defects, particularly those associated with chitin (*CDA2*, *CHS7*, *QRI1*, and CNAG_06898) and glucan biosynthesis (*SKN1*, *KRE6*, *EBG1*, *LPI9*, CNAG_05458, and *BLG2*). Furthermore, genes coding for ER chaperones that aid in protein folding (*ERO1*, *KAR2*, *LHS1*, and *PDI1*) and chaperone regulator (*SCJ1*), and genes involved in proteolysis in the ER (CNAG_04635, CNAG_06658) were induced, likely as part of the ER stress response induced by the accumulation of misfolded proteins in the presence of a defective ERQC.

Further investigation of the effects of *UGG1* disruption in the expression of genes involved in capsule biosynthesis, cell wall remodeling, and the secretion pathways of protein virulence factors using qRT-PCR analysis (Fig. 6D) showed no noticeable changes in the expression of genes related to capsule biosynthesis and conventional or unconventional secretion pathways at mRNA level, despite the aberrantly displayed defective phenotypes.

EV-mediated protein trafficking and non-conventional secretion is impaired in the *ugg1*Δ mutant strain

Many enzymes contribute to the composite cryptococcal virulence phenotype. Some of these virulence-associated enzymes are secreted through traditional secretion pathways, whereas others are packaged into EVs and released into the extracellular milieu via non-conventional secretion mechanisms (Amelida et al., 2015). The defects observed in the ERQC mutant strains, particularly in the production of melanin and polysaccharide capsules, both of which are transported by EVs, suggest a possible impairment in the EV-mediated extracellular transport of virulence-associated enzymes in these mutants. Therefore, we

391 examined the *in vitro* activity of urease, and laccase and acid phosphatase in both intracellular
392 and extracellular fractions.

393 Comparative analysis of the WT and *ugg1*Δ strains showed minimal changes in the
394 intracellular activities of urease, laccase, and acid phosphatase. However, their activities were
395 significantly reduced in the extracellular fractions of the *ugg1*Δ cells (Fig. 7A, 7B, 7C, and
396 7D). Importantly, urease activity was performed in both solid and liquid media,
397 demonstrating a notable loss of secreted urease activity in *ugg1*Δ cells, with a slight decrease
398 in the *mns1*Δ*101*Δ double mutant cells (Fig. 7A and 7B). As urease lacks a signal peptide
399 required for conventional protein secretion, reduced urease secretion strongly indicates a
400 compromised EV-mediated non-conventional secretory pathway in the *ugg1*Δ mutant strain.
401 The decrease in extracellular laccase activity (Fig. 7C) corroborates our melanization assay
402 results, in which *ugg1*Δ showed defective melanin production (Fig. 4A).

403 We next examined cellulase and α-amylase activities to evaluate the impact of ERQC
404 disruption on the conventional secretion pathway of non-virulence-related enzymes (Fig. 7E
405 and 7F). The extracellular activities of these carbohydrate polymer-degrading enzymes in the
406 *ugg1*Δ mutant were slightly lower than those observed in the WT, likely reflecting reduced
407 intracellular enzyme production rather than a substantial impairment of secretion efficiency.
408 Additionally, we analyzed the localization of chitin deacetylase I (Cda1), a
409 glycosylphosphatidylinositol (GPI)-anchored protein involved in converting chitin to chitosan,
410 essential for maintaining cell wall integrity (Baker et al., 2007; Baker et al., 2011; Upadhya et
411 al., 2018; Upadhya et al., 2021). Cda1 was primarily detected in the insoluble cellular protein
412 fraction, encompassing the cell wall and membrane compartments (Fig. 7G, left), consistent
413 with its cell surface localization via a GPI anchor. Cda1 is secreted extracellularly upon
414 cleavage of the GPI anchor. Notably, the *ugg1*Δ mutant exhibited significantly higher
415 intracellular and extracellular Cda1 levels compared to the WT and *mns1*Δ*101*Δ strains (Fig.

7G, right), aligning with a 1.87-fold increase in *CDA1* mRNA expression observed in the RNA-seq data. These findings indicate that the surface localization and secretion of Cda1 remain efficient, suggesting that the conventional secretion pathway is largely unperturbed in *ugg1*Δ. Collectively, these results suggest that while Ugg1-mediated ERQC defects have a pronounced negative effect on EV-mediated protein transport, their impact on the conventional secretion pathway is minimal.

Extracellular vesicle biogenesis and cargo loading are defective in *ugg1*Δ strain

We thus analyzed the number and size distribution of EVs to determine possible abnormal EV-mediated trafficking of virulence factors in the *ugg1*Δ mutant. Nanoparticle tracking analysis (NTA) showed a major peak in size distribution at approximately 150 (134±28) nm in the WT strain, which was similar in size to mammalian exosomes and typical microbial EVs. Additionally, a minor peak ranging from 300–500 nm was observed and corresponded to microvesicles (Fig. 8A). Notably, the size distribution of *ugg1*Δ EVs was more heterogeneous with smaller EVs ranging from 50–150 nm (82±16; 124±14) compared with that of the WT. The *cap59*Δ EVs displayed a major distribution of approximately 150 nm (120±21). Microvesicles were barely detected in either *cap59*Δ or *ugg1*Δ strains.

We observed a significant reduction in the total number of secreted EVs in the *ugg1*Δ mutant (approximately 40%), suggesting defective EV biogenesis and/or stability in the absence of functional Ugg1 (Fig. 8B). Cryo-TEM analysis of EV morphology confirmed that the sizes of EVs released by *ugg1*Δ were significantly smaller and more diverse than those of the WT or the acapsular mutant (Fig. 8C), further supporting the NTA results. Examining EV size distribution by measuring their diameter (Fig. 8D) further confirmed that although the EVs in the WT strain ranged from approximately 50–550 nm in size with distribution

440 primarily concentrated at approximately 150 nm, the EVs in the *ugg1*Δ mutant were smaller
441 (< 100 nm) with heterogeneous sizes. Notably, *cap59*Δ EVs were uniformly distributed at
442 approximately 150 nm and were present at a higher concentration than those of EVs from the
443 WT. An increase in EV release and virulence factors has been also observed in acapsular
444 mutant strains of *C. neoformans* and *C. gattii* (Rodrigues et al., 2007; Reis et al., 2019),
445 supporting the notion that the capsule serves as a barrier in EV release in capsule forming
446 species.

447 To characterize the protein composition of EVs from WT and *ugg1*Δ strains, EV-
448 associated and whole-cell lysate (WCL) proteins were extracted and subjected to proteomic
449 analysis (Fig. 8E). In the WCL, 4,678 proteins were identified in the WT strain, with 333
450 exhibiting differential expression (>2-fold) in *ugg1*Δ versus the WT strain, including 123
451 upregulated and 210 downregulated proteins (Supplementary Fig. S7, A, left). In EVs, 2,075
452 proteins were detected in the WT strain, of which 693 were differentially expressed in EVs
453 from *ugg1*Δ relative to EVs from the WT strain (>2-fold), comprising 273 upregulated and
454 420 downregulated proteins (Supplementary Fig. S7, A, right; Supplementary Table S3).
455 Additionally, comparative proteomic analysis revealed 180 proteins uniquely enriched in EVs
456 (Supplementary Fig. S7, B). The GO enrichment analysis of differentially expressed proteins
457 (> 2-fold) showed distinctive patterns in biological process (BP) and cellular components
458 (CC) between EVs and the WCL (Supplementary Fig. S7, C). Three proteomic analyses of *C.*
459 *neoformans* EVs have been reported previously (Rodrigues et al., 2008; Wolf et al., 2014;
460 Rizzo et al., 2021), identifying 76, 202, and 1,847 proteins associated with EVs, respectively.
461 We compared the EV protein content between WT and *ugg1*Δ identified in our study,
462 focusing on overlapped proteins from the three EV proteomic data sets reported. Among 88
463 commonly reported EV-associated proteins, 29 were downregulated while 16 were

overexpressed in *ugg1*Δ EVs compared to WT EVs (Fig. 8E; Supplementary Table S4). The differential expression pattern of the EV-associated proteins is quite distinctive from that of WCL, revealing significantly detectable changes in EVs. Thus, the absence of functional Ugg1 not only caused morphological alterations and reduced EV numbers but also altered EV protein abundance in *C. neoformans*.

To further examine possible cargo loading defects, we investigated the presence of GXM in the *ugg1*Δ EVs, comparing GXM quantities in the total cell extracts from WT, *ugg1*Δ, and *cap59*Δ strains (Fig. 8F). Cda1 was used as the representative EV-associated protein as its presence was reported within the *C. neoformans* EV membrane, despite a substantial portion of Cda1 being secreted through the conventional secretion pathway (Rizzo et al., 2021). GXM polysaccharides were not detected in the EVs released from *ugg1*Δ, although it was present in the whole-cell extract. Taken together with the reduced quantity of EV-associated proteins, the absence of GXM polysaccharides in *ugg1*Δ EVs strongly indicates that EV cargo loading is defective when the ERQC is dysfunctional in *C. neoformans*.

Discussion

As glycoproteins pass through the ER-Golgi secretory pathway, their *N*-glycans undergo extensive modifications in association with protein quality control. The ERQC system is highly conserved among eukaryotes but also diverged with distinct and species-specific features. The ERQC composition of *C. neoformans* is unique in that it possesses UGGT but lacks the three glucosyltransferases necessary for the addition of glucose residues to the core precursor *N*-glycans (Park et al., 2012). Additionally, it lacks CRT, and carries multiple α1,2-mannosidases. In this study, we investigated the molecular features and functions of the *N*-glycan-dependent ERQC in *C. neoformans*, which generates unique *N*-

glycan precursors without glucose addition, and shorter in length than those of most eukaryotes. Our data strongly suggest that despite the incomplete composition of the ERQC components, the UGGT-centered ERQC plays pivotal roles in cellular fitness, and particularly in the EV-mediated extracellular transport, which is crucial for pathogenicity.

The virulence of the *C. neoformans ugg1*Δ mutant was almost abolished in mice (Fig. 4D), a phenotype consistent with the observed defects in key virulence determinants, such as the capsule and melanin, as well as poor growth at 37 °C (Fig. 3B; Fig. 4A and 4B). The *mns1*Δ*101*Δ mutant displayed intermediate phenotypes between those of the WT and *ugg1*Δ. Our data from the UPR induction analysis and comparative transcriptomic analysis strongly indicate that the ERQC mutation generates ER stress; this accounts for significant similarity of the defective phenotypes of the *C. neoformans* ERQC mutants to those reported in other mutants that exhibit defective protein folding in the ER, particularly in terms of increased stress sensitivity and decreased virulence. Connections between ER stress and thermotolerance have previously been established in *C. neoformans*, as growth at 37 °C requires key ER protein chaperones and protein processing machinery, including components of the UPR signaling pathway Ire1 and the ER stress-responsive transcription factor Hxl1 (Cheon et al., 2011; Havel et al., 2011; Jung et al., 2013). Other mutations causing defects in ER function in *C. neoformans*, such as mutants lacking *DNJ1* (an ER J-domain containing co-chaperone) and *CNE1* (an ER chaperone), resulted in growth inhibition. The *dnj1*Δ mutant strain displayed impaired elaboration of virulence factors, such as the exopolysaccharide capsule and extracellular urease activity, when cultured at human body temperature (Horianopoulos et al., 2021). Altogether with our data from the ERQC mutants, these findings strongly support the notion that maintaining ER homeostasis is crucial for survival and virulence factor production at elevated temperatures.

It is quite notable that the *C. neoformans ugg1*Δ EVs exhibited defective loading of GXM and many protein cargo, alongside a decrease in the number and changes in the size distribution (Fig. 8). Combined with compromised cell fitness, these defects in EV biogenesis and cargo loading, even under normal growth conditions, likely contribute to the complete loss of virulence owing to the defective export of virulence factors in the *ugg1*Δ mutant. Interestingly, our comparative proteome analysis of culture supernatants (secretome) revealed that the *ugg1*Δ strain exhibited more pronounced defects in the secretion of proteins lacking signal peptides, which are often linked to unconventional secretion mechanisms, compared to those with canonical secretion signals (Supplementary Fig. S8; Supplementary Table S5). These findings further support the role of ERQC in modulating non-conventional secretion pathways.

It is intriguing how the absence of Ugg1, leading to ERQC defects, results in defective EV biogenesis and cargo loading in *C. neoformans*. In fungi, EV production and release occur through the maturation of endosomes into multivesicular bodies (MVBs), which are directed to the cell surface. Upon fusion with the plasma membrane, MVBs release vesicles into the extracellular environment, functioning as an unconventional secretion pathway (Oliveira et al., 2010). MVBs formation relies on the functionality of the endosomal sorting complex required for transport (ESCRT), a highly intricate pathway involving a series of finely regulated events (Henne et al., 2011). Deletion of several ESCRT complex-related genes involved in EV transport directly impacts the cryptococcal capsule, notably resulting in reduced capsule size. Specifically, the *C. neoformans vps27*Δ strain showed altered EV size distribution, reduced capsule dimensions, defects in laccase export to the cell wall, and poor extracellular export of urease (Park et al., 2020). Other regulators of unconventional secretion are also linked to EV biogenesis. For example, the Golgi reassembly and stacking proteins (GRASPs) regulate EV cargo and dimensions in *C. neoformans* (Peres et al., 2018). A *grasp*Δ

538 mutant strain produced EVs with dimensions that significantly differed from those produced
539 by WT cells, along with attenuated virulence and abnormal RNA composition. Moreover, the
540 GRASP protein Grasp homology 1 (Grh1) serves as a chaperone that directly influences EV
541 cargo (Malhotra, 2013; Peres da Silva et al., 2018). Autophagy regulators, which participate
542 in EV formation in other eukaryotes, also play a role in cryptococcal EV formation. An *atg7*Δ
543 strain manifests hypovirulence, and EVs produced by this strain show slightly different RNA
544 composition compared with that of the WT cells (Oliveira et al., 2016). Notably, our data of
545 the transcriptome and proteome analysis did not show significant changes in the ESCRT
546 complex and GRASPs.

547 In addition to protein folding and secretion, the ER is crucial for regulating lipid
548 metabolism (Moncan et al., 2021). Consequently, ER stress significantly impacts lipid and
549 sterol synthesis, although some of these mechanisms are yet to be clarified. LDs aid the UPR
550 and ERAD in degrading misfolded proteins during ER stress in *S. cerevisiae* (Garcia et al.,
551 2021). In the present study, we observed a drastic increase in LDs in the *ugg1*Δ mutant
552 (Supplementary Fig. S6, A), consistent with the previous hypothesis that LDs help
553 maintaining ER homeostasis. Furthermore, we observed increased number of vacuoles in
554 *ugg1*Δ (Supplementary Fig. S6, B). This may thus indicate abnormal lipid homeostasis
555 caused by the ERQC defects, which could, in turn, affect EV biogenesis. The importance of
556 lipids and membrane regulators in proper EV formation and GXM export has been suggested
557 in a previous study on the Apt1 flippase in *C. neoformans* (Rizzo et al., 2018). Additionally,
558 ergosterol is essential for membrane fluidity, permeability, and protein transport (Ermakova
559 and Zuev, 2017). Erg6 is involved in the ergosterol biosynthesis pathway and was identified
560 as essential for the trans-Golgi network transport of proteins (Proszynski et al., 2005; Nes et
561 al., 2009). In *C. neoformans*, the *erg6*Δ mutant released EVs with a significantly larger
562 diameter than those of the WT, carrying increased levels of proteins and sterols, highlighting

the role of ergosterol in cryptococcal EV biogenesis (Oliveira et al., 2020). Notably, the *ugg1*Δ mutant exhibited loss of microvesicles, which are derived from the plasma membrane (Fig. 8A). Our preliminary analysis data on the surface lipid fraction of the *ugg1*Δ mutant indicated detectable alteration of sphingolipids and sterol profiles. Altogether, these findings suggest that ER stress caused by misfolded glycoprotein accumulation in ERQC-defective mutants may alter lipid composition, which could affect EV biogenesis.

A recent study using kidney cells presented strong evidence for a key role of ER stress in modulating EV biogenesis, demonstrating that ER stress decreases exosome production in mice (Fukuoka et al., 2023). They showed that T-cadherin is downregulated by ER stress through IRE1α activation at mRNA and protein levels and that ER stress decreases EV production through adiponectin/T-cadherin-independent way, which may involve interferon pathway activation in mice. We similarly observed induced activity of the ER stress sensor Ire1 in *ugg1*Δ, even under normal growth conditions, suggesting a possible association between the Ire1-mediated UPR pathway and EV biogenesis (Fig. 9). Additionally, glycosylation regulates the biogenesis of small EVs and affects protein cargo loading efficiency in melanoma cells (Harada et al., 2020). This suggests that the altered *N*-glycosylation observed in *C. neoformans ugg1*Δ may influence cargo loading of certain EV-targeting glycoproteins. Despite their findings not being conducted in fungi, they provide valuable guides on the investigation of conserved mechanisms shared with *C. neoformans*. Further studies to investigate the mechanisms underlying the ERQC-mediated modulation of EV biogenesis and cargo loading in *C. neoformans* will provide insights into understanding the regulation, production, composition, and diversity of fungal EVs, enabling a better understanding of their biological function. Expanding our knowledge on pathogenic fungal EVs would pave the way for utilizing native or engineered EVs as promising candidates for therapeutic applications, including fungal infection diagnosis and vaccine development.

Materials and Methods

Strains, culture conditions, plasmids, and primers

The *C. neoformans* strains that were constructed and used in this study are listed in Supplementary Table S1A. The plasmids and primers used are listed in Supplementary Tables S1B and S1C, respectively. The construction of the deletion mutants is described in the Supplementary Information. The strains were typically cultured in YPD medium (1% yeast extract, 2% bacto peptone, and 2% glucose) at 30 °C with shaking (220 rpm). *C. neoformans* transformants were selected by culturing on YPD solid medium containing 100 μg/ml nouseothricin acetyltransferase (Jena Bioscience, Germany; indicated as YPD_{NAT}), YPD solid medium with 100 μg/ml hygromycin B (Sigma-Aldrich, USA; indicated as YPD_{HyB}), or YPD solid medium with 100 μg/ml G418 (Duchefa, Netherlands; indicated as YPD_{NEO}). For capsule induction, *C. neoformans* cells were cultured in liquid Sabouraud dextrose medium (Difco) at 30 °C for 16 h and incubated in 10% Sabouraud dextrose medium (pH 7.3) supplemented with 50 mM morpholinepropanesulfonic acid (MOPS) at 30 °C for 2 days. For melanin production analysis, the cells were spotted onto an L-DOPA agar plate (7.6 mM L-asparagine monohydrate, 5.6 mM glucose, 22 mM KH_2PO_4, 1 mM $MgSO_4 \cdot 7H_2O$, 0.5 mM L-DOPA, 0.3 mM thiamine-HCl, and 20 nM biotin) and incubated at 30 °C or 37 °C for 2 days.

Transmission electron microscopy

C. neoformans cells were cultured either at an initial optical density of 600 nm (OD_{600}) of 0.2 at 30 °C in YPD medium until OD_{600} reached 0.8, or for 2 days in 10% Sabouraud media at 30 °C. The cell pellets were washed twice in PBS and fixed for 12 h in 2% glutaraldehyde-2% paraformaldehyde in 0.1 M phosphate buffer (pH 7.4). The cells were washed in 0.1 M phosphate buffer and post-fixed with 1% OsO_4 in 0.1 M phosphate buffer for 2 h. The cells were dehydrated using an ascending ethanol series (50, 60, 70, 80, 90, 95,

100%) for 10 min each and infiltrated with propylene oxide for 10 min. The specimens were embedded with a Poly/Bed 812 kit (Polysciences Inc., USA) and polymerized in an electron microscope oven (TD-700, DOSAKA, Japan) at 65 °C for 12 h. The block was cut into 200-nm semi-thin sections with a diamond knife in the ultramicrotome and stained with toluidine blue for observation using optical microscopy. The region of interest was further cut into 80 nm thin sections using the ultramicrotome, placed on copper grids, double stained with 3% uranyl acetate for 30 min and 3% lead citrate for 7 min, and imaged using a transmission electron microscope (JEM-1011, JEOL, Tokyo, Japan) equipped with a Megaview III CCD camera (Soft imaging system-Germany) at the acceleration voltage of 80 kV.

Capsule transfer and shedding analysis

Capsule transfer assays were performed as described previously (Reese and Doering, 2003). Briefly, conditioned medium (CM) was prepared as a source of GXM by culturing the respective strains for 5 days in YPD medium, followed by filtering and storing the culture supernatant at 4 °C. The acceptor strains were cultured overnight at 30 °C in YPD medium. In total, 2×10^6 acceptor cells were incubated with 1 µl of CM for 1 h at room temperature under rotation (18 rpm) and washed twice with PBS. Capsule acquisition was visualized by incubating the cells with an anti-GXM (18B7) antibody conjugated with AlexaFluor 488 (ThermoFisher Scientific, USA) for 1 h at 37 °C, and observing under an Eclipse Ti-E fluorescence microscope (Nikon, Japan), equipped with a Nikon DS-Qi2 camera. The images were processed using the NIS-elements microscope imaging software (Nikon, Japan). Capsule shedding analysis was performed using a modified previously described protocol (Yoneda and Doering, 2008). The respective strains were cultured in 10% Sabouraud media for 2 days, and the culture supernatant was sterile filtered. Enzyme denaturation was

performed by subjecting the filtrate to heating at 70 °C for 15 min, followed by centrifugation at 13,000 rpm for 3 min. Intracellular GXM analysis was performed by resuspending the pellets in TNE buffer (50 mM Tris-HCl [pH 7.5], 150 mM NaCl, 5 mM EDTA) with the same volume of glass beads (425–600 µm in diameter, Sigma-Aldrich, USA). The cells were disrupted four times for 15 s at 5,000 rpm using a Precellys 24 Tissue Homogenizer (Bertin Technologies, France), followed by centrifugation at 16,000 rpm for 5 min at 4 °C. Next, 10 µl of the supernatant of either secreted or intracellular polysaccharide was mixed with 6X loading dye and run on a 0.6% certified megabase agarose (Bio-rad, USA) gel in 0.5X TBE (44.5 mM Trisma base, 44.5 mM boric acid, 1 mM EDTA [pH 8.0]) at 25 V for 16 h. The polysaccharides were transferred onto a nylon membrane using the southern blotting technique. The membrane was air-dried, blocked using 5% skim milk, and treated overnight with 2 µg/ml 18B7 antibody. After washing, the membrane was incubated with an anti-mouse peroxidase-conjugated secondary antibody and subjected to detection using chemiluminescence.

Detection of enzymatic activities in intracellular and secretary fractions

Biochemical enzymatic activities of acid phosphatase, urease, and laccase in the intracellular and secreted fractions were assayed spectrophotometrically, using previously described methods (Lev et al., 2014; Fu et al., 2018; de Sousa et al., 2022). Acid phosphatase activity was assayed by culturing cells in MM-KCL medium (0.5% KCl, 15 mM glucose, 10 mM $MgSO_4 \cdot 7H_2O$, 13 mM glycine, and 3 µM thiamine) for 3 h at 30 °C. The culture supernatant and soluble cell lysate were allowed to react with 2.5 mM p-nitrophenyl phosphate (pNPP) for 30 min at 37 °C. Urease activity was determined after culturing the cells in Rapid Urea broth (RUH) for 24 h at 30 °C and subjecting the culture supernatant and

soluble cell lysate to incubation with phenol red. Laccase activity was assayed by culturing the cells in asparagine salts media (7.6 mM L-asparagine, 0.1% glucose, 22 mM KH_2PO_4, 1 mM $MgSO_4.7H_2O$, 0.3 mM thiamine-HCl, and 20 nM biotin) for 48 h at 30 °C and allowing the supernatant and soluble cell lysate to react overnight with 10 mM L-DOPA. The reactions were quantified by measuring OD_{420} (acid phosphatase), OD_{570} (urease), or OD_{480} (laccase). Cellulase activity was determined by culturing the cells in cellulose media (0.1% $NaNO_3$, 0.1% K_2HPO_4, 0.1% KCl, 0.5% $MgSO_4$, 0.5% yeast extract, 0.1% glucose, and 0.5% low viscosity carboxymethyl cellulose) for 24 h at 30 °C. The culture supernatants were concentrated using an Amicon tube (30 kDa cutoff, Sigma-Aldrich, USA). The concentrated supernatants and soluble cell lysates were allowed to react at 40 °C for 10 min with the substrate 4,6-O-(3-ketobutylidene)-4-nitrophenyl-β-D-cellopentaoside (BPNPG5), which was provided in the cellulase assay kit (CellG5 Method, Megazyme, Ireland). The reaction was terminated by adding 2% [w/v] Tris buffer (pH 10), and the absorbance of 4-nitrophenol was measured at 400 nm. Cellulase activity (CellG5 Units/ml) was calculated as indicated in the cellulase assay kit. α-amylase activity was measured using the α-Amylase Activity Colorimetric Assay Kit (Biovision Technologies, USA) according to the manufacturer's instructions. Yeast cells were cultured overnight in YPD medium at 30 °C, and the culture supernatants were concentrated using an Amicon tube (30 kDa cutoff, Sigma-Aldrich, USA). The concentrated supernatants and soluble cell lysates were incubated for 1 h at 25 °C in assay buffer with the substrate ethylidene-pNP-G7, which was provided in the kit. OD_{405} was measured. All the activity analysis results were normalized according to cell density (OD_{600}).

Purification, nanoparticle tracking analysis (NTA), and Cryo-TEM imaging of extracellular vesicles

EV purification was performed according to a previously published protocol (Reis et al., 2019) with modifications. One loop of cells was inoculated into 10 ml of liquid YPD and incubated at 30 °C for 24 h with shaking (220 rpm). The cells were washed twice with 10 ml of PBS, counted, and diluted in PBS to a density of 3.5×10^7 cells/ml. Aliquots of cell suspension (300 μl) were spread onto synthetic dextrose (SD) solid medium plates and incubated for 24 h at 30 °C. The cells were carefully recovered from each plate using an inoculation loop, gently resuspended in 30 ml PBS, and pelleted through centrifugation at 4,000 rpm for 10 min at 4 °C. The supernatant was collected and centrifuged again at 15,000 ×*g* for 15 min at 4 °C. Then, the supernatant was filtered through 0.45-μm syringe filters and ultracentrifuged at 100,000 ×*g* for 1 h at 4 °C (MLA-50 fixed angle rotor, Beckman Coulter, Germany). The supernatant was discarded, and the EV pellets were collected and resuspended in 1 ml of PBS for immediate use or stored at -80 °C for further experiments. The samples were diluted 100-fold, and EV sizes were measured using an NTA instrument (NFEC-2024-03-295455, Nanosight Pro, Malvern Panalytical, Netherlands) coupled to a 532-nm laser (Malvern Panalytical, Netherlands), SCMOS camera (Hamamatsu Photonics. Japan), and syringe pump (Malvern Panalytical, Netherlands). The data were analyzed using the NS Xplorer software (v1.1.0.6, Malvern Panalytical, Netherlands).

Cryo-TEM imaging was performed by loading purified EVs (3 μl) onto a lacey carbon grid (Lacey Carbon, 300mesh Cu, Ted Pella Inc., USA), which was glow discharged at 15 mA for 60 s. The sample-loaded grid was blotted for 3 s at 15 °C and 100% humidity and immediately plunge-frozen in liquid ethane. The process was performed by Vitrobot Maek IV (Thermofisher Scientific, USA, SNU, CMCI). The frozen grids were imaged using TEM (JEM-2100F, JEOL, Japan); the temperature of the grid was maintained at approximately -180 °C at an acceleration voltage of 200 keV. The images were recorded

using an ultrascan 1000 electron detector.

Proteomic analysis based on mass spectrometry and data processing

The samples for proteomic analysis were prepared as described in Supplementary Information. The labeled peptides (total, 100 μg proteins) were combined prior to offline basic reverse-phase liquid chromatographic (bRPLC) fractionation. Linear gradient was performed using buffer A (10 mM TEAB in water) and buffer B (10 mM TEAB in 90% acetonitrile), and 10 fractions were analyzed in total using am LC-MS/MS system. The samples were dissolved in 0.1% formic acid using an UltiMate 3000 RSLCnano system and analyzed using an Orbitrap Eclipse Tribrid mass spectrometer (Thermo Fisher Scientific, USA). All MS raw files were converted into mzML and ms2 file formats using the MSConvert (version 3.0.20033) software. The *C. neoformans* proteome was determined by downloading a protein FASTA file from Uniprot (http://uniprot.org), which included 7,492 reviewed (Swiss-Prot) and unreviewed (TrEMBL) proteins entries. A proteome search database with reversed sequence and contaminants in the Integrated Proteomics Pipeline (IP2, version 5.1.2, Integrated Proteomics Applications Inc., San Diego, CA) was generated. The proteome search from 20 ms2 files was performed with IP2 and its following parameters, followed by evaluation for a false discovery rate (FDR) using IP2 and Proteininferencer (version 1.0, Integrated Proteomics Applications Inc., USA). Protein quantification and statistical analysis for discovery of differentially expressed proteins (DEPs) was performed using the ms2 files with tandem mass tag (TMT) reporter ions using an in-house program coded using Python 3.8, where t-test and Pearson's correlation analysis between comparison samples was performed using the scikit-learn (version 0.23.2), Scipy (version 1.6.0), and statsmodels (0.12.1) Python libraries.

Acknowledgments

We thank Arturo Casadevall for providing the 18B7 antibody, Jennifer K. Lodge for providing the anti-Cda1 antibody, and Ji-Yeon Kang for technical assistance with MALDI-TOF analysis.

Competing Interests

The authors declare no conflicts of interest.

Additional information

Funding

This study was supported by the National Research Foundation of Korea (Grant nos. NRF-2022R1A2C1012699, NRF2018R1A5A1025077, and RS-2023-00212663) and by the Korea Institute of Marine Science & Technology Promotion (Grant no. RS-2024-00405273).

Author Contributions

Catia Mota: Investigation, Construction of mutants, Performing all virulence analysis, Data curation, and Writing—original draft; Kiseung Kim: Construction of mutants and Performing phenotype analysis; Ye Ji Son: Transcriptome analysis and Validation; Eun Jung Thak and Su-Bin Lee: Glycan analysis; Ju-El Kim and Jeong-Kee Yoon: NTA analysis; Min-Ho Kang: Cryo-TEM analysis; Heeyoun Hwang: Proteome analysis; Yong-Sun Bahn and J. Andrew

Alspaugh: Supervision, Data curation, Writing—review, and editing; Hyun Ah Kang: Conceptualization, Project administration, Supervision, Data curation, Writing—original draft, review, and editing.

Author ORCIDs

Catia Mota: orcid.org/0009-0001-6129-0000

Ye Ji Son: orcid.org/0009-0006-4324-5800

Eun Jung Thak: orcid.org/0000-0003-4523-142X

Ju-El Kim: orcid.org/0009-0002-3028-1125

Jeong-Kee Yoon: orcid.org/0000-0003-0111-9911

Heeyoun Hwang: orcid.org/0000-0002-0124-2533

Yong-Sun Bahn: orcid.org/0000-0001-9573-5752

J. Andrew Alspaugh: orcid.org/0000-0003-3009-627X

Hyun Ah Kang: orcid.org/0000-0002-3722-525X

Additional files

Supplementary files

Supplementary file 1 – Supplementary material & methods. (a) Construction of *C. neoformans ugg1*Δ and *UGG1* complementation strains. (b) Construction of *C. neoformans mns1*Δ, *mns101*Δ, *mns1*Δ*101*Δ, and respective complementation strains. (c) Construction of *C. neoformans mnl1*Δ, *mnl2*Δ and, *mnl1*Δ*mnl2*Δ strains. (d) Construction and localization analysis of *C. neoformans* GFP-Ugg1, Mns1-GFP, and Mns101-GFP fusion proteins. (e) HPLC and MALDI-TOF-based *N*-glycan structure analysis. (f) Animal study and *in vitro* survival analysis. (g) Subcellular fractionation and western blot analysis of Cda1. (h) RNA

preparation, qRT-PCR, and RNA-sequencing. (i) Sample preparation for proteomic analysis.

Supplementary file 2 - Supplementary figures. (a) Figure S1. Evolutionary conservation and divergence of endoplasmic reticulum quality control (ERQC)-related gene homologues predicted in different eukaryote organisms. (b) Figure S2. Domain analysis of putative *C. neoformans* ERQC-associated proteins. (c) Figure S3. Phenotype characterization of *C. neoformans* α1,2-mannosidases. (d) Figure S4. Subcellular localization of GFP-tagged Ugg1, Mns1, and Mns101. (e) Figure S5. Fungal burden of mice infected with *C. neoformans* ERQC-related mutant cells. (f) Figure S6. Lipid and vacuole staining of WT and *ugg1*Δ strains. (g) Figure S7. Comparative analysis of whole-cell lysate (WCL) and EV proteomes between WT and *ugg1*Δ strains. (h) Figure S8. Comparative analysis of whole-cell lysate (WCL) proteome and secretome between WT and *ugg1*Δ strains.

Supplementary file 3 - Table S1. A. List of strains used in this study; B. List of plasmids used in this study; C. List of primers used in this study.

Supplementary file 4 - Table S2. A. Up-regulated (> 2-fold) *Cryptococcus neoformans* genes in *ugg1*Δ than that of wild type (WT) cultivated in yeast extract peptone dextrose (YPD) at 30 °C, B. Down-regulated (> 2-fold) *Cryptococcus neoformans* genes in *ugg1*Δ than that of wild type (WT) cultivated in YPD at 30 °C.

Supplementary file 5 - Table S3. Excel file containing the list of proteins identified in the proteomic analysis of the wild type (WT) and *ugg1*Δ extracellular vesicles (EVs) and whole-cell lysates (WCL).

Supplementary file 6 - Table S4. Representative extracellular vesicle (EV)-associated proteins commonly detected in this study and previously reported *Cryptococcus neoformans* EV proteome data sets.

Supplementary file 7 - Table S5. Excel file containing the list of proteins identified in the whole-cell lysate (WLC) proteome and secretome analysis in the wild type (WT) and *ugg1*Δ strains.

Data availability

The raw RNA sequencing data have been submitted to the NCBI GEO database under accession no. GSE254772.

References

Aebi M. 2013. *N*-linked protein glycosylation in the ER. *Biochim Biophys Acta*. **1833**: 2430-2437.

Balchin D, Hayer-Hartl M, Hartl FU. 2016. In vivo aspects of protein folding and quality control. *Science* **353**: aac4354.

Baker LG, Specht CA, Donlin MJ, Lodge JK. 2007. Chitosan, the deacetylated form of chitin, is necessary for cell wall integrity in *Cryptococcus neoformans*. *Eukaryot Cell* **6**: 855-867.

Baker LG, Specht CA, Lodge JK. 2011. Cell wall chitosan is necessary for virulence in the opportunistic pathogen *Cryptococcus neoformans*. *Eukaryot Cell* **10**: 1264-1268.

Banerjee S, Vishwanath P, Cui J, Kelleher DJ, Gilmore R, Robbins PW, Samuelson J**.** 2007. The evolution of *N*-glycan-dependent endoplasmic reticulum quality control factors for glycoprotein folding and degradation. *Proc Natl Acad Sci USA* **104**: 11676-11681.

Casadevall A, Coelho C, Cordero RJB, Dragotakes Q, Jung E, Vij R, Wear MP**.** 2019. The capsule of *Cryptococcus neoformans*. *Virulence* **10**: 822-831.

Casadevall A, Cleare W, Feldmesser M, Glatman-Freedman A, Goldman DL, Kozel TR, Lendvai N, Mukherjee J, Pirofski LA, Rivera J, Rosas AL, Scharff MD, Valadon P, Westin K, Zhong Z. 1998. Characterization of a murine monoclonal antibody to *Cryptococcus neoformans* polysaccharide that is a candidate for human therapeutic studies. *Antimicrob Agents Chemother*. **42**:1437-1446.

Chakraborty R, Baek JH, Bae EY, Kim WY, Lee SY, Kim MG. 2016. Comparison and contrast of plant, yeast, and mammalian ER stress and UPR. *Appl Biol Chem.* **59**: 337-347

Chen J, Wen P, Tang YH, Li H, Wang Z, Wang X, Zhou X, Gao XD, Fujita M, Yang G. 2024. Proteome and glycoproteome analyses reveal regulation of protein glycosylation site-specific occupancy and lysosomal hydrolase maturation by *N*-glycan-dependent ER-quality control. *J Proteome Res*. **23**: 4409-4421.

Cheon SA, Jung KW, Chen YL, Heitman J, Bahn YS, Kang HA**.** 2011. Unique evolution of the UPR pathway with a novel bZIP transcription factor, Hxl1, for controlling pathogenicity of *Cryptococcus neoformans*. *PLoS Pathog* **7**: e1002177.

Cowie DB, Cohen GN, Bolton ET, Robichon-Szulmajster H. 1959. Amino acid analog incorporation into bacterial proteins. *Biochim Biophys Acta*. **34**: 39-46.

De Jesus M, Chow SK, Cordero RJ, Frases S, Casadevall A. 2010. Galactoxylomannans from *Cryptococcus neoformans* varieties *neoformans* and *grubii* are structurally and antigenically variable. *Eukaryot Cell*. **9**: 1018-1028.

de Sousa HR, de Oliveira GP Jr, Frazão SO, Gorgonha KCM, Rosa CP, Garcez EM, Lucas J Jr, Correia AF, de Freitas WF, Borges HM, Brito Alves LG, Paes HC, Trilles L, Lazera MDS, Teixeira MM, Pinto VL Jr, Felipe MSS, Casadevall A, Silva-Pereira I, Albuquerque P, Nicola AM. 2022. Faster *Cryptococcus* melanization increases virulence in experimental and human cryptococcosis. *J Fungi* **8**: 393.

Doering TL. 2009. How sweet it is! Cell wall biogenesis and polysaccharide capsule formation in *Cryptococcus neoformans*. *Annu. Rev. Microbiol* **63**: 223-247.

Fu MS, Coelho C, De Leon-Rodriguez CM, Rossi DCP, Camacho E, Jung EH, Kulkarni M, Casadevall A. 2018. *Cryptococcus neoformans* urease affects the outcome of intracellular pathogenesis by modulating phagolysosomal pH. *PLoS Pathog* **14**: e1007144.

Fukuoka K, Mineo R, Kita S, Fukuda S, Okita T, Kawada-Horitani E, Iioka M, Fujii K, Kawada K, Fukushima Y, Nishizawa H, Maeda N, Shimomura L. 2023. ER stress decreases exosome production through adiponectin/T-cadherin-dependent and -independent pathways. *J Biol Chem* **299**: 105-114.

Garcia EJ, Liao PC, Tan G, Vevea JD, Sing CN, Tsang CA, McCaffery JM, Boldogh IR, Pon LA. 2021. Membrane dynamics and protein targets of lipid droplet microautophagy during ER stress-induced proteostasis in the budding yeast, *Saccharomyces cerevisiae*. *Autophagy* **17**: 2363-2383.

Gauss R, Kanehara K, Carvalho P, Ng DT, Aebi M. 2011. A complex of Pdi1p and the mannosidase Htm1p initiates clearance of unfolded glycoproteins from the endoplasmic reticulum. *Mol Cell*. **42**: 782-793.

Grijpstra J, Tefsen B, van Die I, de Cock H. 2009. The *Cryptococcus neoformans* cap10 and cap59 mutant strains, affected in glucuronoxylomannan synthesis, differentially activate human dendritic cells. *FEMS Immunol Med Microbiol* **57**: 142-150.

Gottfredsson M, Perfect JR. 2000. Fungal Meningitis. *Semin. Neurol* **20**: 307-322.

Harada Y, Nakajima K, Suzuki T, Fukushige T, Kondo K, Seino J, Ohkawa Y, Suzuki T, Inoue H, Kanekuta T, Dohmae N, Taniguchi N, Maruyama I. 2020. Glycometabolic regulation of the biogenesis of small extracellular vesicles. *Cell Rep* **33**: 108261.

Havel VE, Wool NK, Ayad D, Downey KM, Wilson CF, Larsen P, Djordjevic JT, Panepinto JC. 2011. Ccr4 promotes resolution of the endoplasmic reticulum stress response during host temperature adaptation in *Cryptococcus neoformans. Eukaryot Cell* **10**: 895–901.

Henne WM, Buchkovich NJ, Emr SD. 2011. The ESCRT pathway. *Dev Cell* **21**: 77-91.

Horianopoulos LC, Lee CWJ, Hu G, Caza M, Kronstad JW. 2021. Dnj1 promotes virulence in *Cryptococcus neoformans* by maintaining robust endoplasmic reticulum homeostasis under temperature stress. *Front Microbiol* **12**: 727039.

Jakob CA, Bodmer D, Spirig U, Battig P, Marcil A, Dignard D, Bergeron JJ, Thomas DY, Aebi M. 2001. Htm1p, a mannosidase-like protein, is involved in glycoprotein degradation in yeast. *EMBO Rep*. **2**: 423-430

Jung KW, Kang HA, Bahn YS. 2013. Essential roles of the Kar2/BiP molecular chaperone downstream of the UPR pathway in *Cryptococcus neoformans*. *PLoS One* **8**: e58956.

Kwon-Chung KJ, Sorrel TC, Dromer F, Fung E, Levitz SM. 2000. Cryptococcosis: clinical and biological aspects. *Med. Mycol* **38**: 205-213

Lee SB, Mota C, Thak EJ, Kim J, Son YJ, Oh DB, Kang HA. 2023. Effects of altered *N*-glycan structures of *Cryptococcus neoformans* mannoproteins, MP98 (Cda2) and MP84 (Cda3), on interaction with host cells. *Sci Rep* **13**: 1175.

Lev S, Crossett B, Cha SY, Desmarini D, Li C, Chayakulkeeree M, Wilson CF, Williamson PR, Sorrel TC, Djordjevic JT. 2014. Identification of Aph1, a phosphate-regulated, secreted, and vacuolar acid phosphatase in *Cryptococcus neoformans*. *mBio* **5**: e01649-14.

Malhotra V. 2013. Unconventional protein secretion: an evolving mechanism. *EMBO J* **32**: 1660-1664.

Marcus NY, Perlmutter DH. 2000. Glucosidase and mannosidase inhibitors mediate increased secretion of mutant alpha1 antitrypsin Z. *J Biol Chem*. **275**:1987-92.

Moncan M, Mnich K, Blomme A, Almanza A, Samali A, Gorman AM. 2021. Regulation of lipid metabolism by the unfolded protein response. *J Cell Mol Med*. **25**: 1359-1370.

Nes WD, Zhou W, Ganapathy K, Liu JL, Vatsyayan R, Chamala S, Hernandez K, Miranda M. 2009. Sterol 24-C-methyltransferase: An enzymatic target for the disruption of ergosterol biosynthesis and homeostasis in *Cryptococcus neoformans*. *Arch. Biochem. Biophys* **481**: 210-218.

Oliveira DL, Nakayasu ES, Joffe LS, Guimarães AJ, Sobreira TJP, Nosanchuk JD, Cordero RJB, Frases S, Casadevall A, Almeida IC, Nimrichter L, Rodrigues ML. 2010. Characterization of yeast extracellular vesicles: evidence for the participation of different pathways of cellular traffic in vesicle biogenesis. *PLoS ONE* **5**: e11113.

Oliveira DL, Fonseca FL, Zamith-Miranda D, Nimrichter L, Rodrigues J, Pereira MD, Reuwsaar JC, Schrank A, Staats C, Kmetzsch L, Vainstein MH, Rodrigues ML. 2016. The putative autophagy regulator Atg7 affects the physiology and pathogenic mechanisms of *Cryptococcus neoformans*. *Future Microbiol* **11**: 1405-1419.

Oliveira FFM, Paes HC, Peconick LDF, Fonseca FL, Marina CLF, Bocca AL, Homem-de-Mello M, Rodrigues ML, Albuquerque P, Nicola AM, Alspaugh JA, Felipe MSS, Fernandes L. 2020. Erg6 affects membrane composition and virulence of the human fungal pathogen *Cryptococcus neoformans*. *Fungal Genet. Biol* **140**: e103368.

O'Meara TR, Norton D, Price MS, Hay C, Clements MF, Nichols CB, Alspaugh JA. 2010. Interaction of *Cryptococcus neoformans* Rim101 and protein kinase A regulates capsule. *PLoS Pathogens* **6**: e1000776.

Park JN, Lee DJ, Kwon O, Oh DB, Bahn YS, Kang HA. 2012. Unraveling unique structure and biosynthesis pathway of *N*-linked glycans in human fungal pathogen *Cryptococcus neoformans* by glycomics analysis. *J Biol Chem* **287**: 19501–19515.

Park YD, Chen SH, Camacho E, Casadevall A, Williamson PR. 2020. Role of the ESCRT pathway in laccase trafficking and virulence of *Cryptococcus neoformans*. *Infect Immun* **88**: e00954-19.

Peres da Silva R, Martins SDT, Rizzo J, Dos Reis FCG, Joffe LS, Vainstein M, Kmetzsch L, Oliveira DL, Puccia R, Goldenberg S, Rodrigues ML, Alves LR. 2018. Golgi reassembly and stacking protein (GRASP) participates in vesicle-mediated RNA export in *Cryptococcus neoformans*. *Genes* **9**: 400.

Ploegh HL. 2007. A lipid-based model for the creation of an escape hatch from the endoplasmic reticulum. *Nature* **448**: 435–438.

Proszynski TJ, Klemm RW, Gravert M, Hsu PP, Gloor Y, Wagner J, Kozak K, Grabner H, Walzer K, Bagnat M, Simons K, Walch-Solimena C. 2005. A genome-wide visual screen reveals a role for sphingolipids and ergosterol in cell surface delivery in yeast. *Proc. Natl. Acad. Scie. U.S.A* **102**: 32201128.

Qiu Y, Davis M.J, Dayrit JK, Hadd Z, Meister DL, Osterholzer JJ, Williamson PR, Olszewski MA. 2012. Immune modulation mediated by cryptococcal laccase promotes pulmonary growth and brain dissemination of virulent *Cryptococcus neoformans* in mice. *PLoS ONE* **7**: e47853.

Rapoport TA. 2007. Protein translocation across the eukaryotic endoplasmic reticulum and bacterial plasma membranes. *Nature* **450**: 663-669.

Reis FCG, Borges BS, Jozefowicz LJ, Sena BAG, Garcia AWA, Medeiros LC, Martins ST, Honorato L, Schrank A, Vainstein MH, Kmetzsch L, Nimrichter L, Alves LR, Staats CC, Rodrigues ML. 2019. A novel protocol for the isolation of fungal extracellular vesicles reveals the participation of a putative scramblase in polysaccharide export and capsule construction in *Cryptococcus gattii*. *mSphere* **4**: e00080-19.

Rizzo J, Wong SSW, Gazi AD, Moyrand F, Chaze T, Commere PH, Novault S, Matondo M, Péhau-Arnaudet G, Reis FCG, Vos M, Alves LR, May RC, Nimrichter L, Rodrigues ML,

Aimanianda V, Janbon G. 2021. *Cryptococcus* extracellular vesicles properties and their use as vaccine platforms. *J Extracell Vesicles* **10**: e12129.

Rizzo J, Colombo AC, Zamith-Miranda D, Silva VKA, Allegood JC, Casadevall A, Del Poeta M, Nosanchuk JD, Kronstad JW, Rodrigues ML. 2018. The putative flippase Apt1 is required for intracellular membrane architecture and biosynthesis of polysaccharide and lipids in *Cryptococcus neoformans*. *Biochim Biophys Acta Mol Cell Res* **1865**: 532-541.

Reese AJ, Doering TL. 2003. Cell wall alpha-1,3-glucan is required to anchor the *Cryptococcus neoformans* capsule. *Mol. Microbiol.* **50**: 1401–1409.

Rodrigues ML, Nimrichter L, Oliveira DL, Frases S, Miranda K, Zaragoza O, Alvarez M, Nakouzi A, Feldmesser M, Casadevall A. 2007. Vesicular polysaccharide export in *Cryptococcus neoformans* is a eukaryotic solution to the problem of fungal trans-cell wall transport. *Eukaryot Cell* **6**: 48–59.

Rodrigues ML, Nakayasu ES, Oliveira DL, Nimrichter L, Nosanchuk JD, Almeida IC, Casadevall A. 2008. Extracellular vesicles produced by *Cryptococcus neoformans* contain protein components associated with virulence. *Eukaryot Cell* **7**: 58–67.

Samuelson J, Banerjee S, Magnelli P, Cui J, Kelleher DJ, Gilmore R, Robbins PW. 2005. The diversity of dolichol-linked precursors to Asn-linked glycans likely results from secondary loss of sets of glycosyltransferases. *Proc Natl Acad Sci USA* **102**: 1548-1553.

Samuelson J, Robbins PW. 2015. Effects of *N*-glycan precursor length diversity on quality control of protein folding and on protein glycosylation. *Semin Cell Dev Biol.* **41**: 121-128.

Singh A, Panting RJ, Varma A, Saijo T, Waldron KJ, Jong A, Ngamskulrungroj P, Chang YC, Rutherford JC, Kwon-Chung KJ. 2013. Factors required for activation of urease as a virulence determinant in *Cryptococcus neoformans*. *mBio* **4**: e00220-13.

Thak EJ, Kim J, Lee DJ, Kim JY, Kang HA. 2018. Structural analysis of *N*-/*O*-glycans assembled on proteins in yeasts. *J Microbiol* **56**: 11–23.

Thak EJ, Lee SB, Xu-Vanpala S, Lee DJ, Chung SY, Bahn YS, Oh DB, Shinohara ML, Kang HA. 2020. Core *N*-glycan structures are critical for the pathogenicity of *Cryptococcus neoformans* by modulating host cell death. *mBio* **11**: e00711-00720.

Thak EJ, Son YJ, Lee DJ, Kim H, Kim JH, Lee SB, Jang YB, Bahn YS, Nichols CB, Alspaugh JA, Kang HA. 2022. Extension of *O*-linked mannosylation in the Golgi apparatus is critical for cell wall integrity signaling and interaction with host cells in *Cryptococcus neoformans* pathogenesis. *mBio* **13**: e0211222.

Thibault G, Ng DT. 2012. The endoplasmic reticulum-associated degradation pathways of budding yeast. *Cold Spring Harb Perspect Biol*. **4**: a013193.

Trotter EW, Kao CM, Berenfeld L, Botstein D, Petsko GA, Gray JV. 2002. Misfolded proteins are competent to mediate a subset of the responses to heat shock in *Saccharomyces cerevisiae*. *J Biol Chem*. **277**: 44817-44825.

Upadhya R, Baker LG, Lam WC, Specht CA, Donlin MJ, Lodge JK. 2018. *Cryptococcus neoformans* Cda1 and its chitin deacetylase activity are required for fungal pathogenesis. *mBio*. **9**: e02087-18.

Upadhya R, Lam WC, Hole CR, Parchment D, Lee CK, Specht CA, Levitz SM, Lodge JK. 2021. *Cryptococcus neoformans* Cda1 and Cda2 coordinate deacetylation of chitin during infection to control fungal virulence. *Cell Surf* **7**: 100066.

Varki A. (2017) Biological roles of glycans. *Glycobiology*. **27**:3-49.

Vevea JD, Garcia EJ, Chan RB, Zhou B, Schultz M, Di Paolo G, McCaffery JM, Pon LA. 2015. Role for lipid droplet biogenesis and microlipophagy in adaptation to lipid imbalance in yeast. *Dev Cell* **35**: 584–599.

Wolf JM, Espadas-Moreno J, Luque-Garcia JL, Casadevall A. 2014. Interaction of *Cryptococcus neoformans* extracellular vesicles with the cell wall. *Eukaryot Cell* **13**: 1484-1493.

Yoneda A, Doering TL. 2006. A eukaryotic capsular polysaccharide is synthesized intracellularly and secreted via exocytosis. *Mol Biol Cell* **17**: 5131–5140.

Yoneda A, Doering TL. 2008. Regulation of *Cryptococcus neoformans* capsule size is mediated at the polymer level. *Eukaryot Cell* **7**: 546–549.

Xu C, Ng DT. 2015. Glycosylation-directed quality control of protein folding. *Nat Rev Mol Cell Biol* **16**: 742-752.

Figure legends

Figure 1. **Presence of UDP-glucose:glycoprotein glucosyltransferase (UGGT) and α1,2-mannosidases as endoplasmic reticulum protein quality control (ERQC) components in *Cryptococcus neoformans*.** (A) Schematic representation of the ERQC pathway in *Homo sapiens, Saccharomyces cerevisiae*, and *Cryptococcus neoformans*. In mammals, the oligosaccharyltransferase (OST) complex attaches $Glc_3Man_9GlcNAc_2$ to nascent polypeptides, followed by glucose trimming by glucosidases I and II (GLS1/GLS2). This generates $Glc_1Man_9GlcNAc_2$, which binds to calnexin (CNX) or calreticulin (CRT) for folding. UGGT reglucosylates misfolded proteins, allowing refolding, while properly folded proteins undergo mannose trimming by ERMan I before Golgi transport. In contrast, fungal ERQC systems differ in key components. *S. cerevisiae* lacks UGGT, relying instead on Gls1/Gls2 and calnexin (Cne1). *C. neoformans* possesses UGGT but lacks ER glucosyltransferases (Alg6, Alg8 and Alg19) and CRT, resulting in a distinct ERQC system. (B) Domain structures of proteins encoded by *C. neoformans UGG1* (CNAG_03648), *MNS1* (CNAG_02081), *MNS101* (CNAG_03240), *MNL1* (CNAG_01987), and *MNL2* (CNAG_04498).

Figure 2. *N*-glycan profile analysis of *C. neoformans* ERQC mutant strains. The HPLC and MALDI-TOF-based *N*-glycan structure analysis were carried out as described in Supplementary information. (A) HPLC-based analysis of *N*-glycan profiles of the *ugg1*Δ mutant. (B) Lectin blotting of sodium dodecyl sulphate (SDS)-polyacrylamide gels containing intracellular or secreted proteins into the culture supernatants of the wild type (WT) and *ugg1*Δ strains. Yeast cells were cultivated in YPD medium for 24 h, harvested, and subjected to sample preparation of soluble intracellular proteins and secreted proteins. The

proteins (30 μg) were loaded on 15% SDS-polyacrylamide gel and analyzed using silver staining (left) or blotting (right) with *Galanthus nivalis* agglutinin (Roche), which recognizes terminal α1,2-, α1,3-, and α1,6-linked mannose residues. (C) HPLC analysis of total *N*-glycan profiles of *mns1*Δ, *mns101*Δ, and *mns1*Δ*101*Δ mutants. (D) MALDI-TOF profiles of neutral *N*-glycans of *mns1*Δ, *mns101*Δ, and *mns1*Δ*101*Δ mutants. The *N*-glycans of cell wall mannoproteins from *C. neoformans* cells were AA-labelled and analyzed using HPLC. For MALDI-TOF analysis, neutral *N*-glycan fractions were obtained from the HPLC fractionation of total *N*-glycans.

Figure 3. Growth phenotype of *C. neoformans* ERQC mutant strains. (A) Expression analysis of ERQC genes in *C. neoformans*. Yeast cells were cultured in YPD medium to a mid-logarithmic phase and exposed to dithiothreitol (DTT; 20 mM), tunicamycin (TM; 5 μg/ml) or cultured at 37 °C for 1 h. The relative transcript levels of *C. neoformans* genes were analyzed using qRT-PCR and normalized with that of *ACT1*. Error bars represent standard deviation of duplicated assays. All statistical data were determined based on one-way ANOVA and Dunnett's post-hoc test. *** $P < 0.0005$, ** $P < 0.003$, *** $P < 0.005$, * $P < 0.05$. (B) Spotting analysis of *C. neoformans ugg1*Δ mutant strains under various stress conditions such as heat stress (37 °C and 39 °C), ER stress (DTT and TM), cell-wall stress (CFW: calcofluor white, CR: Congo red, SDS: Sodium dodecyl sulfate, caffeine), osmotic stress (NaCl, KCl, sorbitol) and treatment with antifungal drugs (fluconazole, ketoconazole, fludioxonil). (C) Growth analysis in the presence of 5',5',5'-trifluoroleucine (TFL). Respective strains were spotted on SC-Leucine media with or without TFL supplementation. Plates were incubated for 3 days at 30 °C. (D) RT-PCR analysis of *IRE1*-dependent splicing of *HXL1*. Strains were cultured in YPD supplemented with 5 μg/ml TM.

Figure 4. *In vitro* and *in vivo* virulence-associated phenotypes of *C. neoformans UGG1, MNS1,* and *MNS101* mutant strains. (A) Melanin synthesis analysis on L-DOPA plates. WT, *ugg1*Δ, *ugg1*Δ*::UGG1*, *mns1*Δ, *mns101*Δ, *mns1*Δ*101*Δ, *mns1*Δ*101*Δ*::MNS1*, *mns1*Δ*101*Δ*::MNS101*, and *cac1*Δ (negative control) strains were serially diluted, plated on L-DOPA plates, and incubated at 30 °C and 37 °C. (B) Melanin synthesis activity per cell of the *ugg1*Δ mutant. WT, *ugg1*Δ, *ugg1*Δ*::UGG1 w*ere cultured in liquid L-DOPA medium. The amount of melanin in the culture supernatant was measured and normalized by cell density. (C) Capsule formation. Cells were cultured for 2 days in 10% Sabouraud media at 30 °C and observed under the microscope. Statistical significance: ****, $P < 0.0001$, ns, not significant). (D) *In vivo* virulence analysis. A/Jcr mice (n=8) were infected with 10^5 cells of WT, *ugg1*Δ, and *ugg1*Δ*::UGG1*, *mns1*Δ, *mns101*Δ, *mns1*Δ*101*Δ, *mns1*Δ*101*Δ*::MNS1*, and *mns1*Δ*101*Δ*::MNS101* strains, and survival was monitored for 2 months, as described in the Supplementary Information. (E) Survival of *C. neoformans* in macrophages. Survival of *C. neoformans* cells within the J774A.1 macrophage-like cell line was determined by counting colony formation unit (CFU) obtained from lysed macrophages from two biologically independent experiment sets. **** $P < 0.0001$, *** $P < 0.0005$, * $P < 0.05$, ns, not significant. All statistical data were determined based on one-way ANOVA and Dunnett's post-hoc test.

Figure 5. Capsule shedding and transfer analysis of *C. neoformans UGG1, MNS1,* and *MNS101* mutant strains. (A) Capsule shedding analysis. The presence of intracellular (left) and shed (right) glucuronoxylomannan (GXM) was assessed by blotting a cell culture filtrate using the monoclonal antibody 18B7. The arrow indicates the direction of electrophoresis. (B) Capsule transfer analysis using exogenous capsule material from WT. The capsule transfer assay was performed using the indicated strains as acceptors. Surface capsules were probed

using the anti-GXM antibody 18B7 conjugated with AlexaFluor 488. Quantitative measurement of fluorescence intensity was calculated based on independent triplicate experiments with standard deviations presented as error bars. (C) Capsule transfer analysis using exogenous capsule material from WT or *mns1*Δ*101*Δ. Statistical significance: **** $P < 0.0001$. All statistical data were determined based on one-way ANOVA and Dunnett's post-hoc test. (D) Transmission electron microscopy (TEM) of *C. neoformans* WT, *ugg1*Δ, and *mns1*Δ*101*Δ strains. Yeast cells were grown overnight at 30 °C in YPD medium and fixed in 2% glutaraldehyde and 2% paraformaldehyde. A Zeiss Axioscope (A1) equipped with an AxioCan MRm digital camera was used to visualize India ink-stained *C. neoformans* cells. Specimens were prepared using critical point drying prior to TEM microscopy. Capsule and yeast cell body diameters were measured using ImageJ (National Institute of Health).

Figure 6. Transcriptome analysis of *C. neoformans* WT and *ugg1*Δ cells. (A) Volcano plot comparing a 2-fold differential gene expression between *ugg1*Δ and WT strains under normal growth conditions. (B) Number of genes upregulated and downregulated by ≥ 2-fold in *ugg1*Δ compared with that of the WT. (C) Gene ontology (GO) analysis of differentially expressed genes between WT and *ugg1*Δ strains. Significantly upregulated genes in *ugg1*Δ are shown in red, whereas significantly downregulated genes in *ugg1*Δ are shown in blue. Total RNA was extracted and subjected to RNAseq analysis as described in the Supplementary Information. (D) qRT-PCR analysis of mRNA expression levels of a set of genes responsible for capsule biosynthesis, cell wall remodeling, and both conventional and non-conventional secretion in *ugg1*Δ vs WT under normal growth conditions from three biologically independent experiment sets.

Figure 7. Analysis of protein secretion in *C. neoformans UGG1, MNS1,* and *MNS101* mutant strains. (A) Spot assay for urease analysis on Christensen's urea agar. Absence of pink coloration indicates loss of urease activity. (B, C, D) Analysis of secretion for virulence-related enzymes such as urease, laccase, and acid phosphatase from three biologically independent experiment sets. Statistical significance: **** $P < 0.0001$, ** $P < 0.003$, *** $P < 0.005$, * $P < 0.05$. All statistical data were determined based on one-way ANOVA and Dunnett's post-hoc test. (E, F) Analysis of secretion for non-virulence-related enzymes such as cellulase and α-amylase. Statistical significance: *** $P<0.0005$, ** $P<0.003$ * $P < 0.05$, ns, not significant. All statistical data were determined based on one-way ANOVA and Dunnett's post-hoc test. (G) Analysis of the conventional secretion of Cda1 in *C. neoformans*. Presence of Cda1 was analyzed in total (T), soluble (S), and insoluble (I) fractions of intracellular extracts (left), along with the secreted fraction (right). Subcellular fractionations were performed as previously described (Thak et al., 2022), and the fractions were subjected to western blotting analysis using an anti-Cda1 antibody.

Figure 8. Analysis of extracellular vesicles purified from WT, *ugg1*Δ, and *cap59*Δ cells. (A, B) Nanoparticle tracking analysis (NTA) of EVs extracted from WT, *ugg1*Δ, and *cap59*Δ strains and quantification of total extracellular vesicle (EV) concentration per cell density. Quantitative measurements were derived from three independent experiments with standard deviations presented as error bars. Statistical significance: *** $P<0.0005$, * $P< 0.05$. All statistical data were determined based on one-way ANOVA and Dunnett's post-hoc test. (C, D) Cryo-TEM imaging of purified EVs and comparative analysis of EV size in WT, *ugg1*Δ, and *cap59*Δ strains. Scale bar, 100 nm. The outer EV diameter of a total number of 100 EVs per strain, captured using cryo-TEM, were measured. (E) Heatmap representation of fold change

between WT and *ugg1*Δ EV-associated proteins, commonly detected in this study and in previously reported EV proteome datasets (*ugg1*Δ/WT). Upregulated proteins in *ugg1*Δ are shown in red, whereas downregulated proteins are shown in blue. The proteome data of whole-cell lysates (WCL), generated from the cell pellets obtained after EV separation, were included for comparison. (F) Blotting analysis of GXM in the *C. neoformans* cells and EVs of WT, *ugg1*Δ, and *cap59*Δ strains. The 8 M urea extracts were obtained from EVs and cell pellets, from which EVs are generated. The urea extracts (5 μg total proteins) were loaded on 8% SDS-polyacrylamide gel and subjected to silver staining or blotting analysis using the anti-GXM 18B7 (α-GXM) and anti-Cda1 (α-Cda1) antibodies, respectively. Left: total cell extract. Right: total EV extract.

Figure 9. Impact of ERQC disruption on glycoprotein folding and EV-mediated transport of virulence factors in *C. neoformans*. (A) In WT strain, *C. neoformans* UGGT homolog, Ugg1, functions as a sensor for misfolded glycoproteins within the ER, playing a crucial role in protein quality control. Functional ERQC is essential not only for ensuring the proper folding of glycoproteins, which is critical for maintaining cellular fitness, but also for facilitating EV-mediated secretion of capsule polysaccharides and virulence-related enzymes necessary for pathogenicity. (B) In the UGGT-deficient strain (*ugg1*Δ), ER stress is increased because of misfolded protein accumulation within the ER lumen. This heightened stress leads to decreased cellular fitness, which negatively impacts EV biogenesis and cargo loading. Consequently, significant defects occur in EV-mediated transport, which ultimately leads to a complete loss of virulence. Nc: nucleus, Vc: vacuoles. This figure was partially created using BioRender.

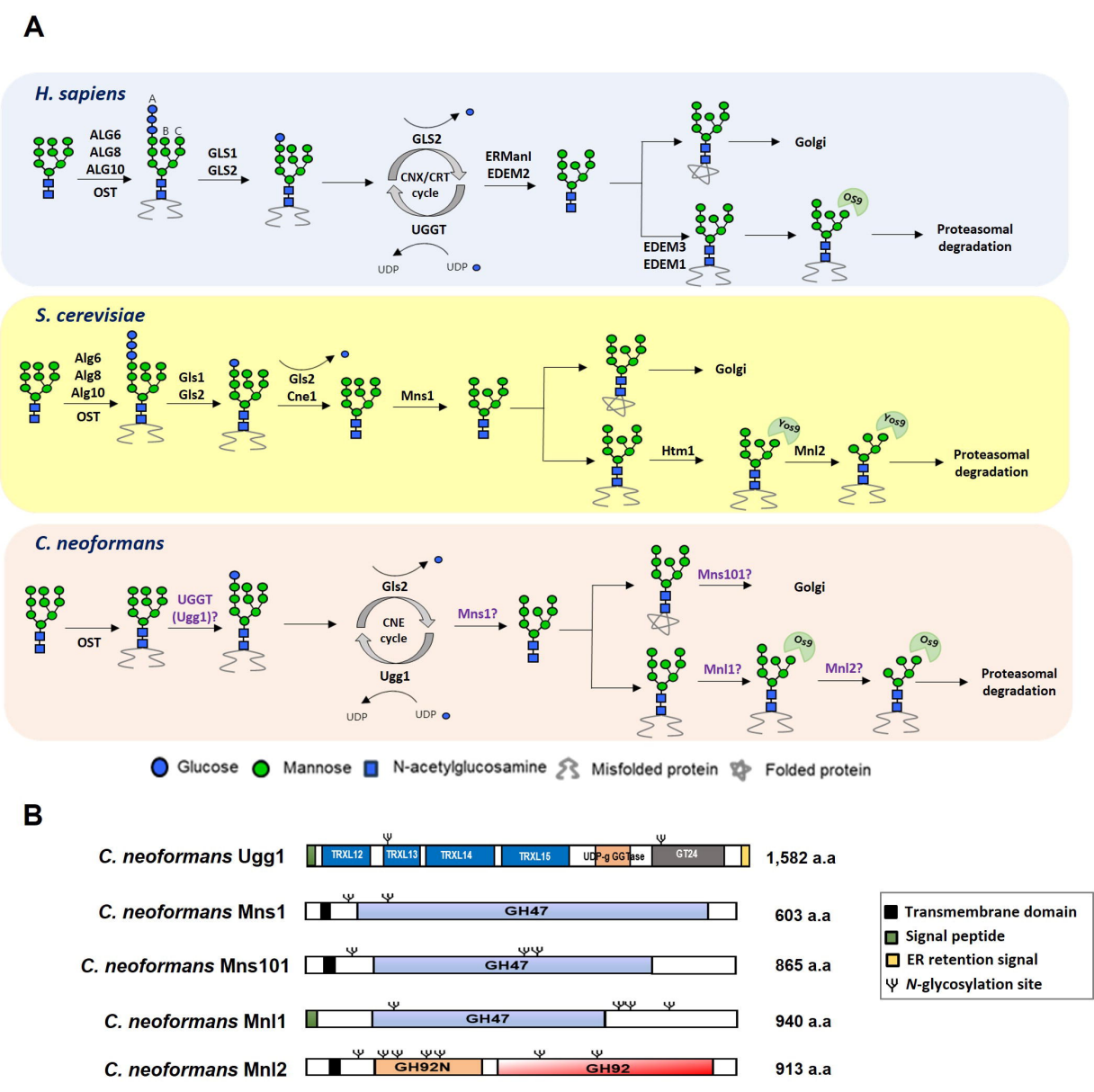
A
H. sapiens
ALG6
ALG8
ALG10
OST
A
B C
GLS1
GLS2
GLS2
CNX/CRT
cycle
UGGT
UDP
UDP
ERManI
EDEM2
Golgi
EDEM3
EDEM1
Osg
Proteasomal
degradation
S. cerevisiae
Alg6
Alg8
Alg10
OST
Gls1
Gls2
Gls2
Cne1
Mns1
Golgi
Htm1
Yos9
Mnl2
Yos9
Proteasomal
degradation
C. neoformans
OST
UGGT
(Ugg1)?
Gls2
CNE
cycle
Ugg1
UDP
UDP
Mns1?
Mns101?
Golgi
Mnl1?
Osg
Mnl2?
Osg
Proteasomal
degradation
Glucose
Mannose
N-acetylglucosamine
Misfolded protein
Folded protein
B
C. neoformans Ugg1
TRXL12
TRXL13
TRXL14
TRXL15
UDP-g GGTase
GT24
1,582 a.a
C. neoformans Mns1
GH47
603 a.a
C. neoformans Mns101
GH47
865 a.a
C. neoformans Mnl1
GH47
940 a.a
C. neoformans Mnl2
GH92N
GH92
913 a.a
Transmembrane domain
Signal peptide
ER retention signal
N-glycosylation site

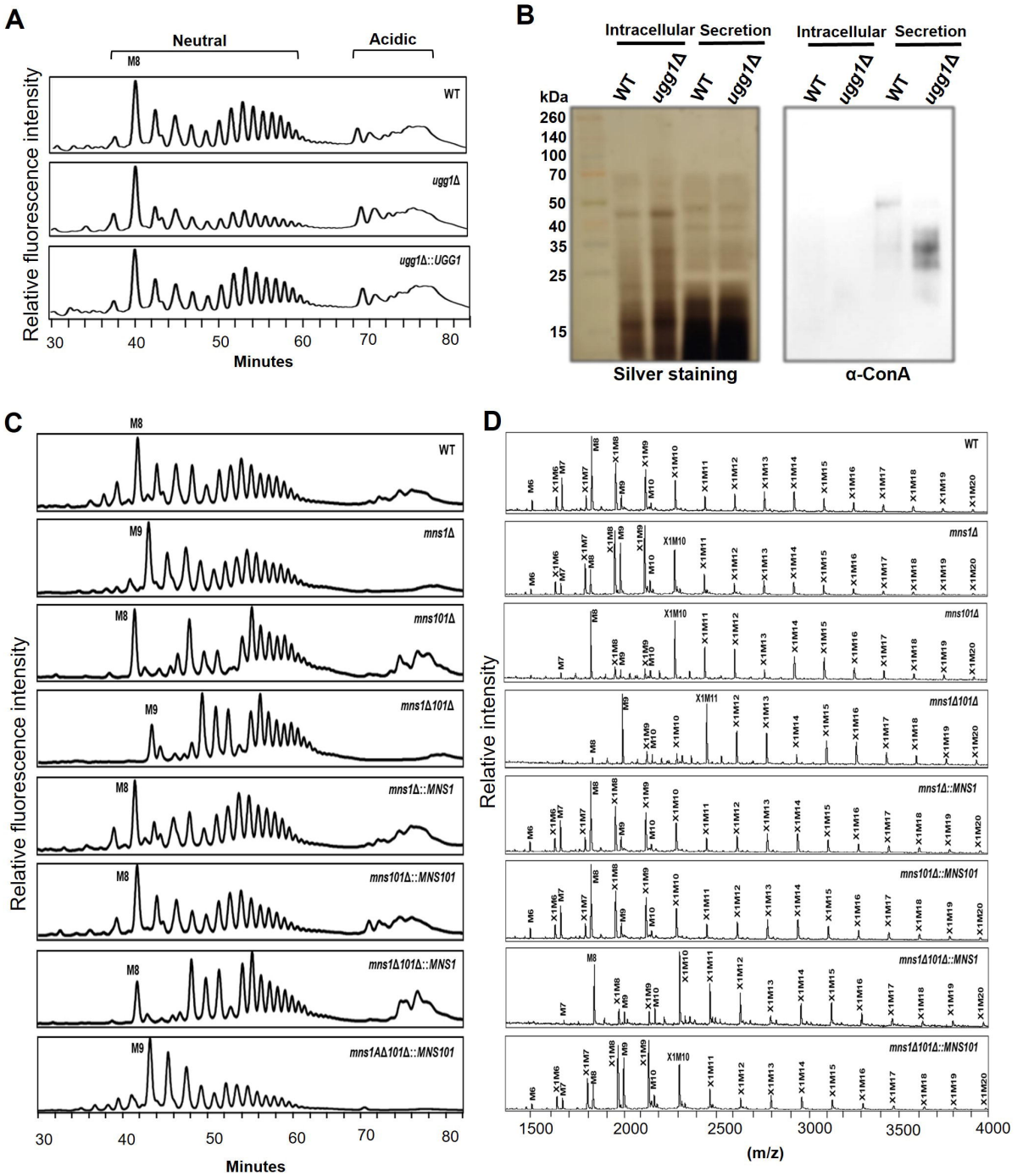
A
Neutral
Acidic
M8
WT
ugg1Δ
ugg1Δ::UGG1
Relative fluorescence intensity
30
40
50
60
70
80
Minutes
B
Intracellular
Secretion
WT
ugg1Δ
kDa
260
140
100
70
50
40
35
25
15
Silver staining
α-ConA
C
M8
M9
mns1Δ
mns101Δ
mns1Δ101Δ
mns1Δ::MNS1
mns101Δ::MNS101
mns1Δ101Δ::MNS1
mns1AΔ101Δ::MNS101
Relative fluorescence intensity
Minutes
D
M6
M7
X1M6
X1M7
X1M8
X1M9
X1M10
X1M11
X1M12
X1M13
X1M14
X1M15
X1M16
X1M17
X1M18
X1M19
X1M20
Relative intensity
1500
2000
2500
3000
3500
4000
(m/z)

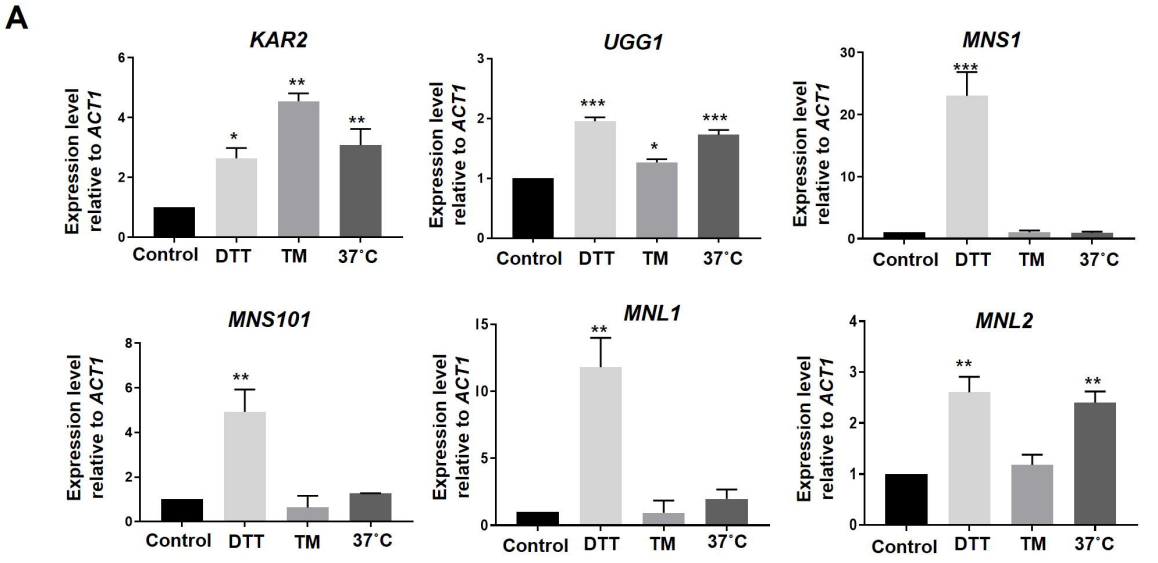
A
KAR2
UGG1
MNS1
MNS101
MNL1
MNL2
Expression level relative to ACT1
Control
DTT
TM
37°C

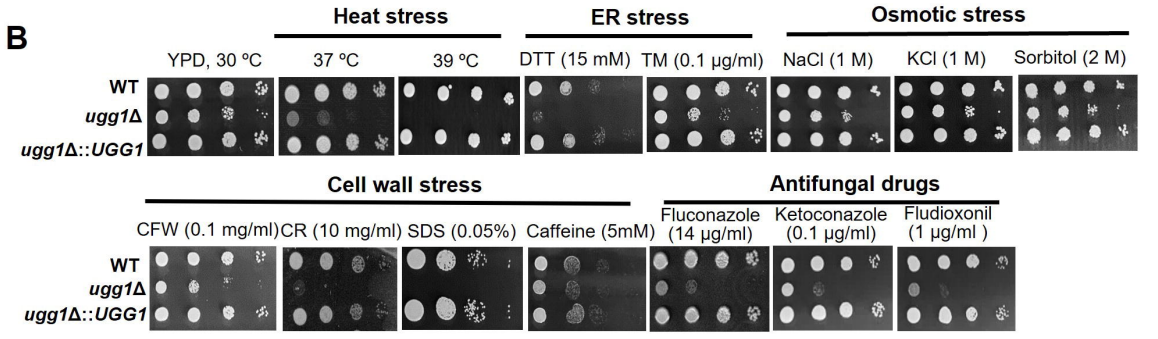
B
Heat stress
ER stress
Osmotic stress
YPD, 30 ºC
37 ºC
39 ºC
DTT (15 mM)
TM (0.1 µg/ml)
NaCl (1 M)
KCl (1 M)
Sorbitol (2 M)
WT
ugg1Δ
ugg1Δ::UGG1
Cell wall stress
Antifungal drugs
CFW (0.1 mg/ml)
CR (10 mg/ml)
SDS (0.05%)
Caffeine (5mM)
Fluconazole (14 µg/ml)
Ketoconazole (0.1 µg/ml)
Fludioxonil (1 µg/ml)

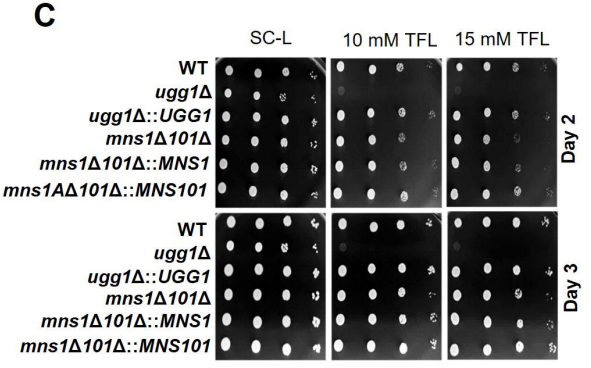
C
SC-L
10 mM TFL
15 mM TFL
WT
ugg1Δ
ugg1Δ::UGG1
mns1Δ101Δ
mns1Δ101Δ::MNS1
mns1AΔ101Δ::MNS101
Day 2
Day 3

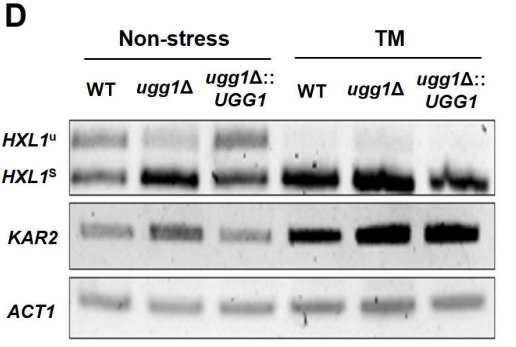
D
Non-stress
TM
WT
ugg1Δ
ugg1Δ::UGG1
HXL1u
HXL1S
KAR2
ACT1

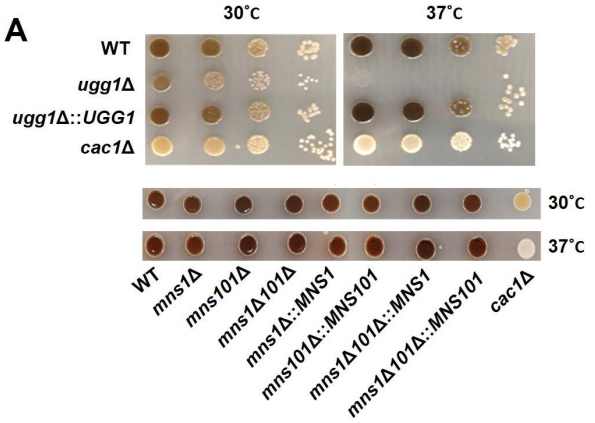
A
30°C
37°C
WT
ugg1Δ
ugg1Δ::UGG1
cac1Δ
30°C
37°C
WT
mns1Δ
mns101Δ
mns1Δ101Δ
mns1Δ::MNS1
mns101Δ::MNS101
mns1Δ101Δ::MNS1
mns1Δ101Δ::MNS101
cac1Δ

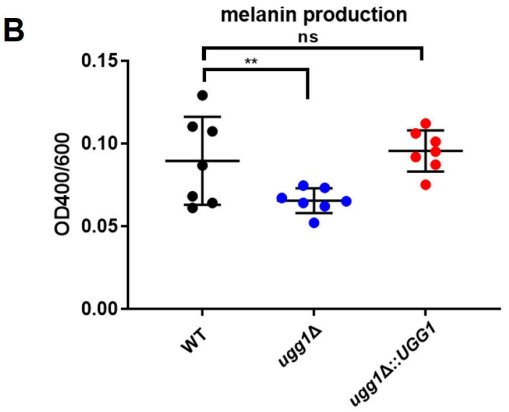
B
melanin production
ns
**
OD400/600
0.15
0.10
0.05
0.00
WT
ugg1Δ
ugg1Δ::UGG1

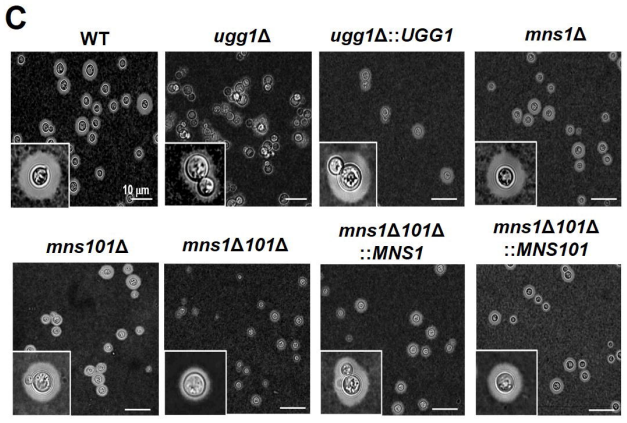
C
WT
ugg1Δ
ugg1Δ::UGG1
mns1Δ
10 μm
mns101Δ
mns1Δ101Δ
mns1Δ101Δ
::MNS1
mns1Δ101Δ
::MNS101

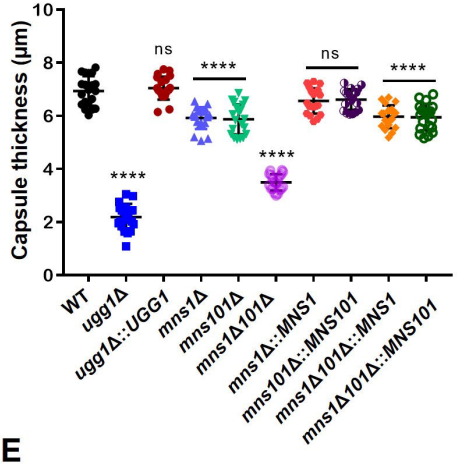
Capsule thickness (μm)
10
8
6
4
2
0
****
ns
****
****
ns
****
WT
ugg1Δ
ugg1Δ::UGG1
mns1Δ
mns101Δ
mns1Δ101Δ
mns1Δ::MNS1
mns101Δ::MNS101
mns1Δ101Δ::MNS1
mns1Δ101Δ::MNS101

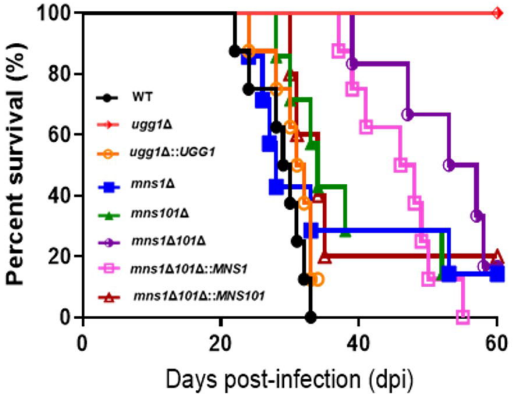
D
Percent survival (%)
100
80
60
40
20
0
0
20
40
60
Days post-infection (dpi)
WT
ugg1Δ
ugg1Δ::UGG1
mns1Δ
mns101Δ
mns1Δ101Δ
mns1Δ101Δ::MNS1
mns1Δ101Δ::MNS101

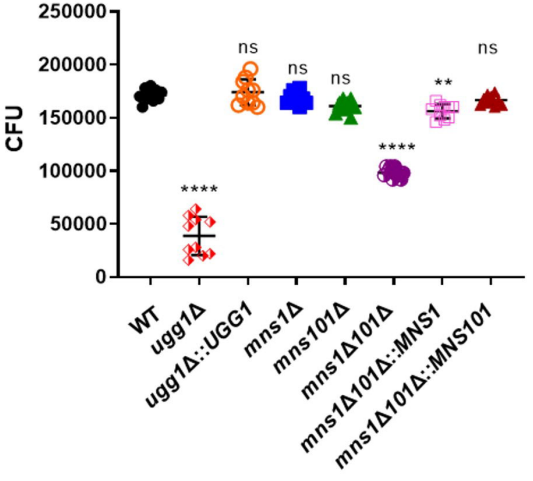
E
CFU
250000
200000
150000
100000
50000
0
****
ns
ns
ns
****
**
ns
WT
ugg1Δ
ugg1Δ::UGG1
mns1Δ
mns101Δ
mns1Δ101Δ
mns1Δ101Δ::MNS1
mns1Δ101Δ::MNS101

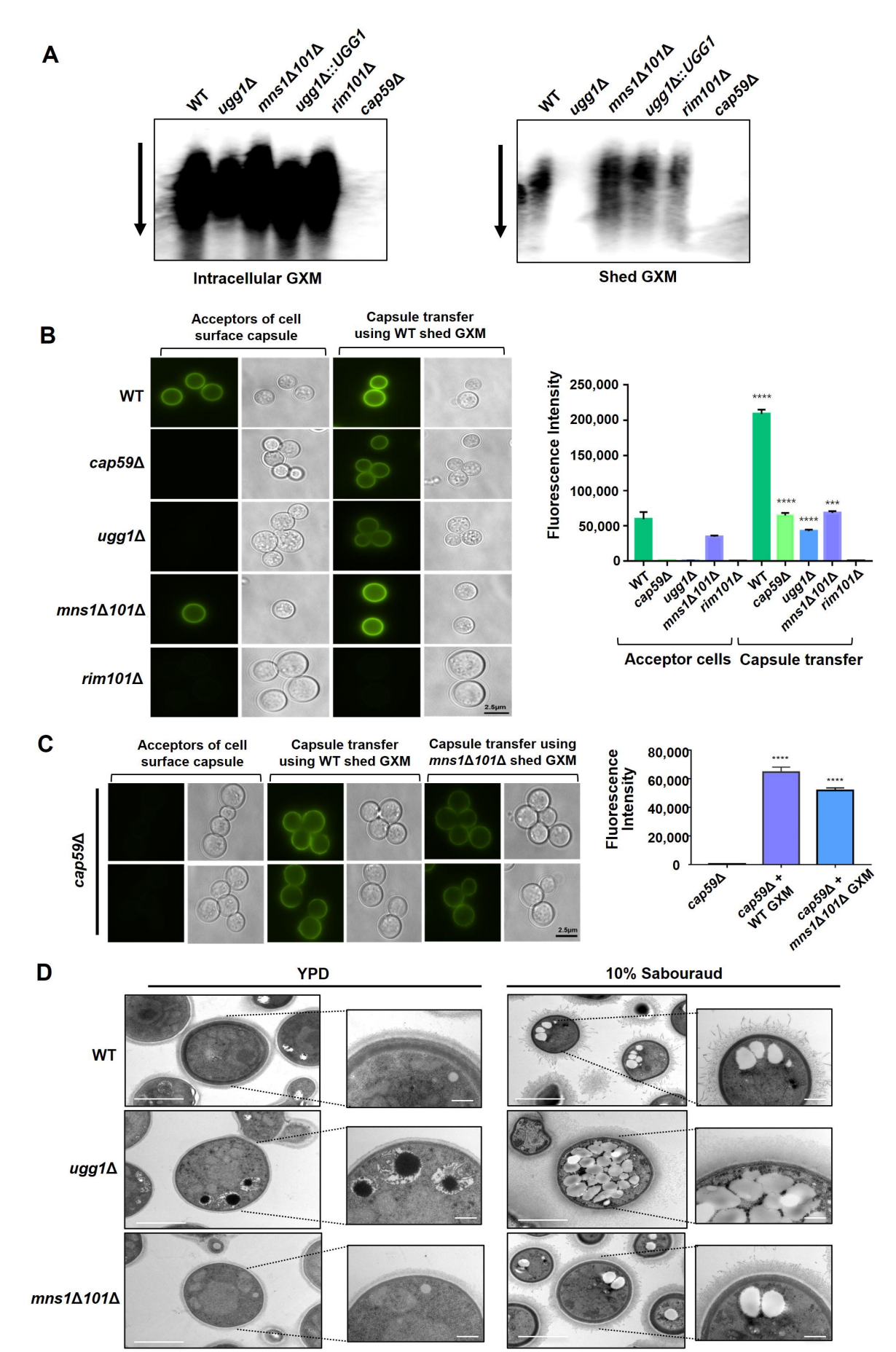
A
WT
ugg1Δ
mns1Δ101Δ
ugg1Δ::UGG1
rim101Δ
cap59Δ
Intracellular GXM
Shed GXM
B
Acceptors of cell surface capsule
Capsule transfer using WT shed GXM
WT
cap59Δ
ugg1Δ
mns1Δ101Δ
rim101Δ
2.5μm
Fluorescence Intensity
250,000
200,000
150,000
100,000
50,000
0
****
***
Acceptor cells
Capsule transfer
C
Acceptors of cell surface capsule
Capsule transfer using WT shed GXM
Capsule transfer using mns1Δ101Δ shed GXM
cap59Δ
2.5μm
Fluorescence Intensity
80,000
60,000
40,000
20,000
0
cap59Δ
cap59Δ + WT GXM
cap59Δ + mns1Δ101Δ GXM
D
YPD
10% Sabouraud
WT
ugg1Δ
mns1Δ101Δ

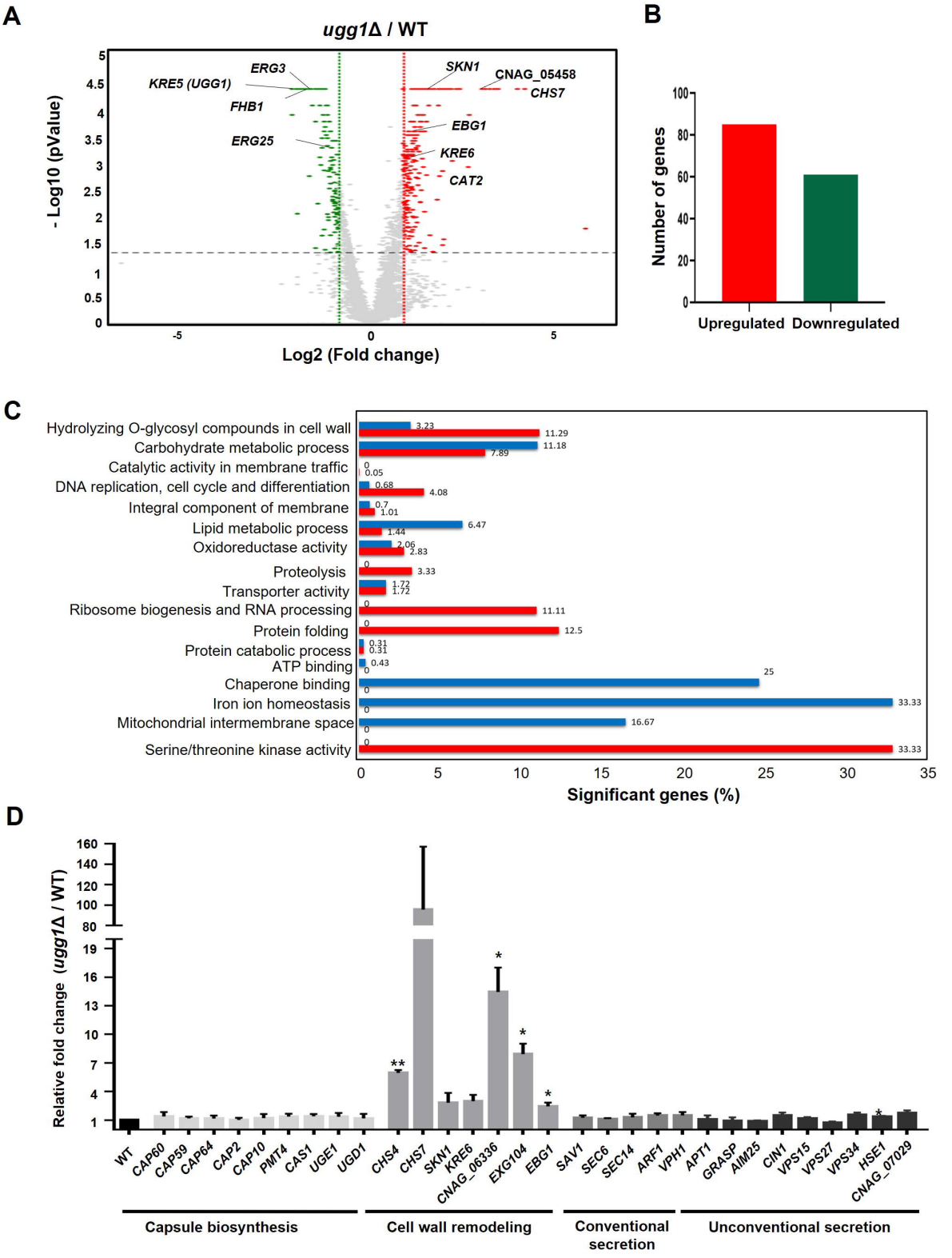
A
ugg1Δ / WT
- Log10 (pValue)
Log2 (Fold change)
ERG3
KRE5 (UGG1)
FHB1
ERG25
SKN1
CNAG_05458
CHS7
EBG1
KRE6
CAT2
B
Number of genes
Upregulated
Downregulated
C
Hydrolyzing O-glycosyl compounds in cell wall
Carbohydrate metabolic process
Catalytic activity in membrane traffic
DNA replication, cell cycle and differentiation
Integral component of membrane
Lipid metabolic process
Oxidoreductase activity
Proteolysis
Transporter activity
Ribosome biogenesis and RNA processing
Protein folding
Protein catabolic process
ATP binding
Chaperone binding
Iron ion homeostasis
Mitochondrial intermembrane space
Serine/threonine kinase activity
Significant genes (%)
D
Relative fold change (ugg1Δ / WT)
WT
CAP60
CAP59
CAP64
CAP2
CAP10
PMT4
CAS1
UGE1
UGD1
CHS4
CHS7
SKN1
KRE6
CNAG_06336
EXG104
EBG1
SAV1
SEC6
SEC14
ARF1
VPH1
APT1
GRASP
AIM25
CIN1
VPS15
VPS27
VPS34
HSE1
CNAG_07029
Capsule biosynthesis
Cell wall remodeling
Conventional secretion
Unconventional secretion

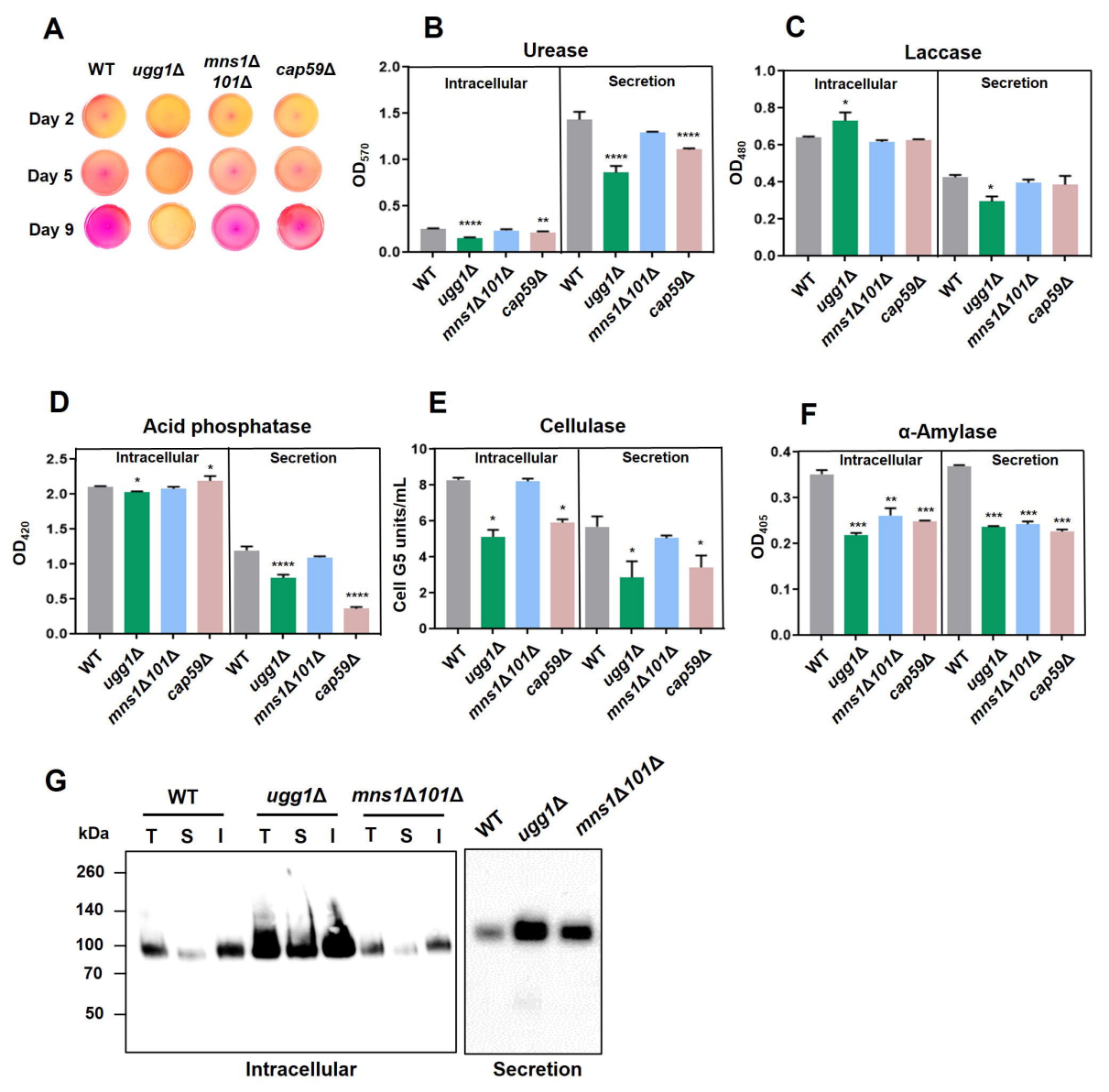
A
WT
ugg1Δ
mns1Δ 101Δ
cap59Δ
Day 2
Day 5
Day 9
B
Urease
Intracellular
Secretion
OD570
C
Laccase
OD480
D
Acid phosphatase
OD420
E
Cellulase
Cell G5 units/mL
F
α-Amylase
OD405
G
kDa
T S I
260
140
100
70
50
Intracellular
Secretion

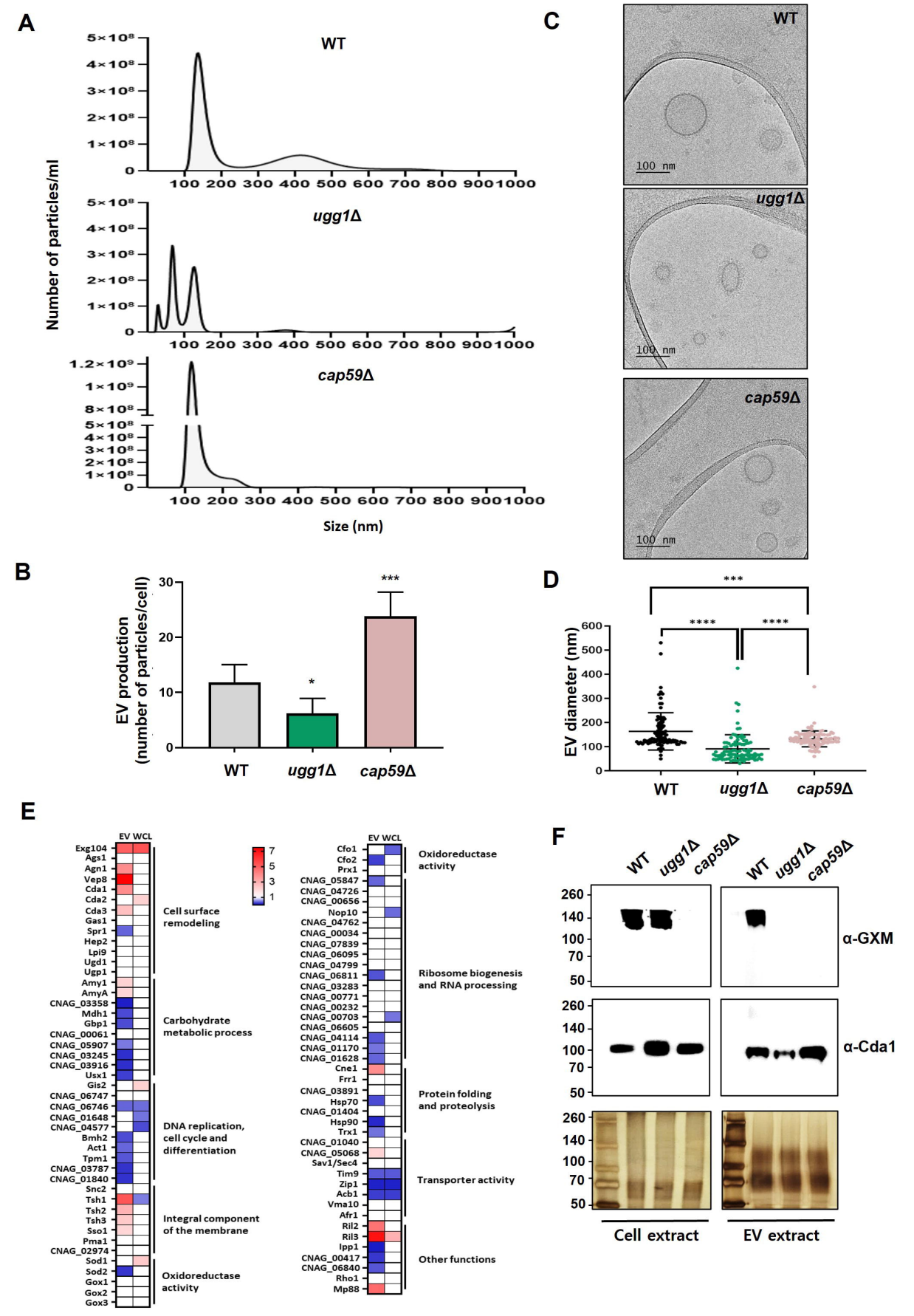
A
WT
ugg1Δ
cap59Δ
Number of particles/ml
Size (nm)
B
EV production (number of particles/cell)
WT
ugg1Δ
cap59Δ
C
WT
ugg1Δ
cap59Δ
100 nm
D
EV diameter (nm)
WT
ugg1Δ
cap59Δ
E
EV WCL
Cell surface remodeling
Carbohydrate metabolic process
DNA replication, cell cycle and differentiation
Integral component of the membrane
Oxidoreductase activity
Ribosome biogenesis and RNA processing
Protein folding and proteolysis
Transporter activity
Other functions
F
WT
ugg1Δ
cap59Δ
α-GXM
α-Cda1
Cell extract
EV extract

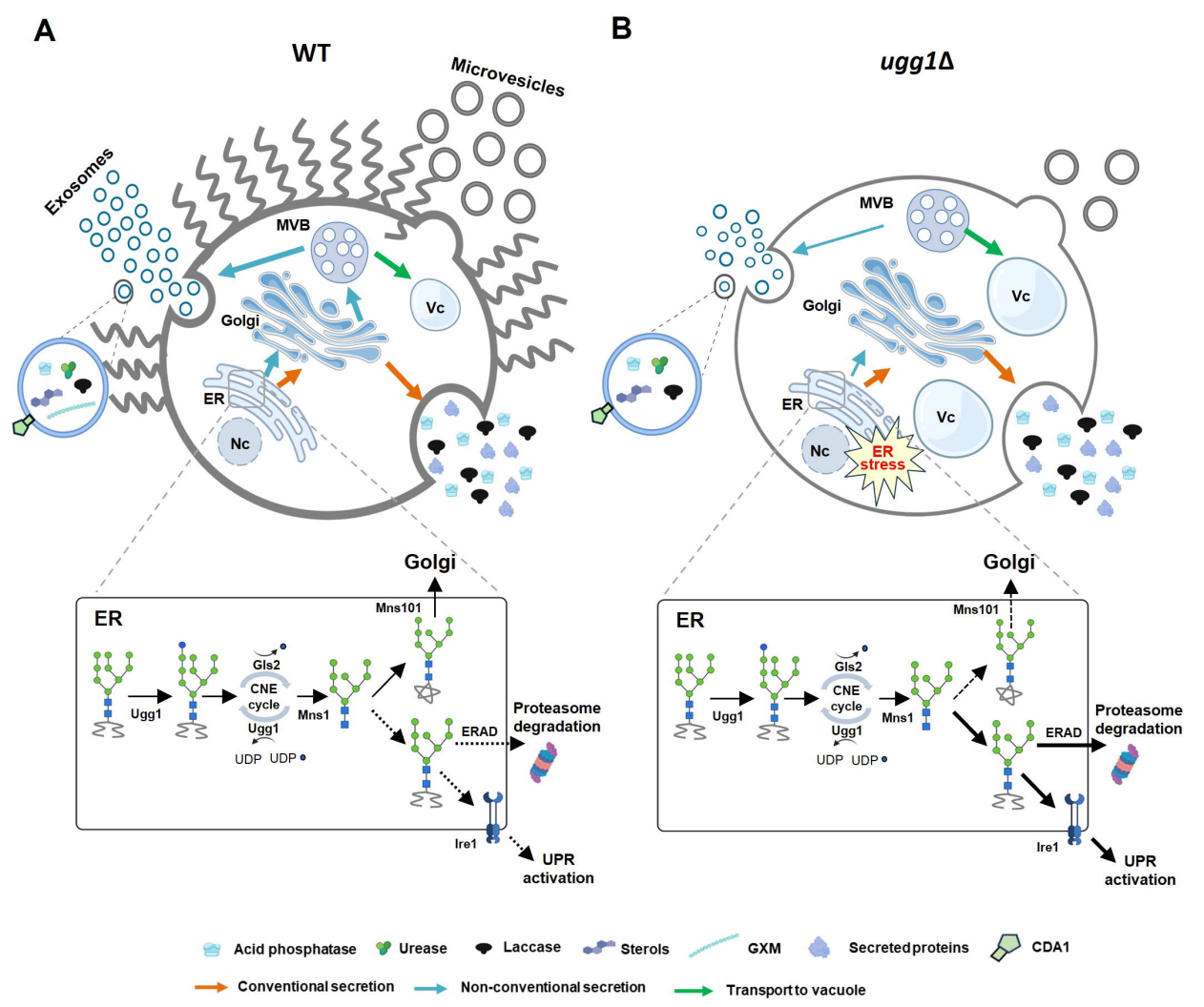
A
WT
Microvesicles
Exosomes
MVB
Golgi
Vc
ER
Nc
Golgi
ER
Mns101
Gls2
CNE cycle
Ugg1
Mns1
Ugg1
UDP UDP
ERAD
Proteasome degradation
Ire1
UPR activation
B
ugg1Δ
MVB
Golgi
Vc
ER
Vc
Nc
ER stress
Golgi
ER
Mns101
Gls2
CNE cycle
Ugg1
Mns1
Ugg1
UDP UDP
ERAD
Proteasome degradation
Ire1
UPR activation
Acid phosphatase
Urease
Laccase
Sterols
GXM
Secreted proteins
CDA1
Conventional secretion
Non-conventional secretion
Transport to vacuole